The Dynamics and Coarsening of Interfaces for the Viscous Cahn-Hilliard Equation in One Spatial Dimension

Xiaodi Sun and Michael J. Ward[1]
Department of Mathematics, University of British Columbia
Vancouver, B.C. V6T 1Z2, Canada

Abstract

In one spatial dimension, the metastable dynamics and coarsening process of an n-layer pattern of internal layers is studied for the Cahn-Hilliard equation, the viscous Cahn-Hilliard equation, and the constrained Allen-Cahn equation. These models from the continuum theory of phase transitions provide a caricature of the physical process of the phase separation of a binary alloy. A homotopy parameter is used to encapsulate these three phase separation models into one parameter-dependent model. By studying a differential-algebraic system of ordinary differential equations describing the locations of the internal layers for a metastable pattern for this parameter-dependent model, we are able to provide detailed comparisons between the internal layer dynamics for the three models. Layer collapse events are studied in detail and the analytical theory is supplemented by numerical results showing the different behaviors for the different models. Finally, an asymptotic-numerical algorithm, based on our asymptotic information of layer collapse events and the conservation of mass condition, is devised to characterize the entire coarsening process for each of these models. Numerical realizations of this algorithm are shown.

1 Introduction

Numerous attempts have been made in recent years to characterize the dynamics of phase separation in binary alloys. When a binary alloy, composed of species A and B, is prepared in a state of isothermal equilibrium at a temperature T_1, greater than the critical temperature T_c, the alloy's composition is spatially uniform with a given concentration u, of B. When the two component system is quenched (rapidly cooled) to a uniform temperature T_2 less that T_c, the cooled system will separate itself out into a coexistence of two phases with a spatial pattern composed of "grains" rich in either A or B. This pattern then undergoes a coarsening or ripening process on a slower time scale, as the system losses some of the grains, tending toward more stable patterns.

In the context of the continuum theory of phase transitions, one of the simplest models to characterize this process in one spatial dimension is the Cahn-Hilliard equation [8]

$$u_t = -\left(\varepsilon^2 u_{xx} + Q(u)\right)_{xx} , \tag{1.1}$$

[1]This work was supported by NSERC grant 5-81541

with homogeneous boundary conditions for u_x and u_{xxx} at $x = \pm 1$. The nonlinearity $Q(u)$ is the derivative of a double-well potential $V(u)$ with wells of equal depth. We assume that $Q(u)$ has exactly three zeros on the interval $[s_-, s_+]$, located at $u = s_- < 0$, $u = 0$ and $u = s_+ > 0$, with

$$Q'(s_\pm) < 0\,, \quad Q'(0) > 0\,, \quad \text{and} \quad V(s_+) = 0\,, \quad \text{where} \quad V(u) \equiv -\int_{s_-}^{u} Q(\eta)\, d\eta\,. \tag{1.2}$$

Prototypical is $Q(u) = 2(u - u^3)$, for which $s_\pm = \pm 1$ and $V(u) = (1-u^2)^2/2$. In (1.1), $\varepsilon \ll 1$ measures the thickness of an interface separating the two preferred states s_+ and s_- of the system, and the term $-\varepsilon^2 u_{xxxx}$ represents a gradient energy regularization of the ill-posed problem $u_t = -[(Q(u)]_{xx}$. From a material science viewpoint, (1.1) is very primitive in that it neglects anisotropic effects, viscous stresses, etc. As shown in [18], and the references therein, when the viscous stresses arising from the relative fluxes of the two components are taken into account, the Cahn-Hilliard equation (1.1) gets modified to the viscous Cahn-Hilliard equation

$$u_t = -\left(\varepsilon^2 u_{xx} + Q(u) - \kappa u_t\right)_{xx}\,, \tag{1.3}$$

with the same boundary conditions. Here the term κu_{xxt}, with $\kappa > 0$ represents a viscous stress regularization. Although these models still only provide, at best, a caricature of the physical coarsening process for a binary alloy, they are mathematically very intricate. As an alternative to these more complicated models, another phase separation called the constrained Allen-Cahn equation, was introduced in [21]. It is given by

$$u_t = \varepsilon^2 u_{xx} + Q(u) - \frac{1}{2}\int_{-1}^{1} Q(u)\, dx\,, \tag{1.4}$$

with homogeneous Neumann conditions at $x = \pm 1$. For each of these models (1.1), (1.3) and (1.4), the mass is conserved. The well-known Allen-Cahn equation, which does not conserve mass, is given by (1.4) with the non-local term in (1.4) omitted.

In our one-dimensional setting, the dynamics associated with these models is expected to proceed in two stages when ε is small: a relatively fast stage during which a pattern of internal layers is formed from initial data in an $O(1)$ time interval, followed by an exponentially slow, or metastable, coarsening process during which the internal layers move exponentially slowly in time until they collapse together in pairs or against the endpoints. This eventually leads to a stable equilibrium solution over an exponentially long time interval.

In the pioneering work of [9] and [13], a system of differential equations characterizing the metastable dynamics of the internal layer motion for the Allen-Cahn equation was derived rigorously. A formal asymptotic analysis was previously given in [17]. The coarsening process for the Allen-Cahn equation, and some generalizations, was described quantitatively in [22]. For the more difficult Cahn-Hilliard equation (1.1), numerical results illustrating a similar slow coarsening behavior were given in [11], [16], and [5]. A hybrid

method to simulate the coarsening process for (1.1) was described in [12]. The existence of metastable dynamics for (1.1) was then proved in [1], [7], [6], and [14]. However, the work of [6] is more explicit, in the sense that an explicit set of differential equations for the metastable internal layer motion was derived. For the viscous Cahn-Hilliard equation, some numerical results for the coarsening behavior and the structure of the attractor were described in [4], although no explicit characterization of the metastable dynamics was obtained. There have been no detailed studies of the coarsening behavior of a metastable pattern for (1.4).

The primary purpose of this paper is to systematically compare and contrast the dynamics and the coarsening process of an n-layer metastable pattern for the three phase separation models (1.1), (1.3) and (1.4). A very convenient way to analyze these models simultaneously is to introduce a homotopy parameter α satisfying $0 \le \alpha \le 1$. Then, in terms of α we write the viscous Cahn-Hilliard equation in the form

$$(1-\alpha)u_t = -\left(\varepsilon^2 u_{xx} + Q(u) - \alpha\kappa u_t\right)_{xx} , \quad -1 < x < 1 , \quad t > 0 , \tag{1.5a}$$

$$u_x(\pm 1, t) = u_{xxx}(\pm 1, t) = 0 ; \quad u(x,0) = u_0(x) . \tag{1.5b}$$

We assume below that the initial data $u_0(x)$ is such that the mass $m \equiv \int_{-1}^{1} u\,dx$ satisfies $s_- < m < s_+$. Then, the mass is conserved in time. The importance of the homotopy parameter α is to distinguish three cases: (i) $\alpha = 0$, (ii) $0 < \alpha < 1$, $\kappa \neq 0$ and (iii) $\alpha = 1$, $\kappa \neq 0$. In case (i), (1.5) reduces to the Cahn-Hilliard equation (1.1). In case (iii), we can integrate the right side of (1.5a) twice, explicitly impose a mass constraint, and then re-scale t to obtain the constrained Allen-Cahn equation (1.4). Case (ii) corresponds to the viscous Cahn-Hilliard equation (1.3). Thus, the homotopy parameter α enables us to understand how the three different models are related by studying only (1.5). A differential-algebraic (DAE) system of equations for the evolution of the internal layer locations of a metastable pattern for (1.5) was derived in [20] using a formal asymptotic method. However, since the system is rather complicated, only the simplest case of a two-layer evolution was studied in [20].

To study the metastable dynamics of an n-layer pattern for (1.5) with $n > 2$ we begin with the DAE system as derived in [20]. In the limit $\varepsilon \to 0$, we can asymptotically reduce this system to show that there are essentially only two ranges of α where the behavior differs: the viscous range $0 < \alpha \le 1$ and the Cahn-Hilliard equation $\alpha = 0$. The existence of these two main ranges of α was also found in [4], where the regularity and smoothness properties of solutions to (1.5) was studied. The DAE system is then used to explain quantitatively the prominent features of the solution observed in the full numerical simulations for various values of α. Therefore, we supplement the analysis by showing full numerical results for the solution to the different models during various types of layer collapse events. A novel procedure to obtain these numerical results, which uses a transverse methods of lines approach, is described. By studying the dynamics of layer collapse events in detail, we are able to devise a hybrid asymptotic-numerical algorithm,

based on our asymptotic information and the conservation of mass condition, to characterize the entire coarsening process for each of these models.

The organization of this paper is as follows. In §2 we introduce our notation, and briefly outline the derivation of the DAE system for the metastable dynamics of (1.5) as derived in [20]. We also describe our numerical procedure for computing solutions to (1.5). In §3, we asymptotically reduce the DAE system for the metastable dynamics in the limit $\varepsilon \to 0$ for the viscous parameter range $0 < \alpha \leq 1$ and for the Cahn-Hilliard equation $\alpha = 0$. In §4, we compare and contrast the dynamics of layer collapse events for both of these ranges of α. It is shown that layer collapse events for the Cahn-Hilliard equation differ substantially from those of (1.5) when $0 < \alpha \leq 1$. For the Cahn-Hilliard equation, we also comment on the relationship between our results and those in [6]. Finally, in §5 we devise an interface realignment algorithm, based on the results in §4, to simulate the entire coarsening process associated with the various phase separation models. Numerical results from this algorithm are given.

2 The Metastability Analysis and the Numerical Method

In this section we introduce some notation and outline the derivation given in [20] of the ODE system describing the metastable evolution of n internal layers for (1.5). For the analysis, it is convenient to rewrite (1.5) in terms of the unknowns $u(x,t)$ and $\sigma(x,t)$ as

$$\alpha\kappa u_t = \varepsilon^2 u_{xx} + Q(u) - \sigma\,, \qquad u_x(\pm 1,t) = 0\,, \tag{2.1a}$$

$$(1-\alpha)u_t = -\sigma_{xx}\,, \qquad \sigma_x(\pm 1,t) = 0\,. \tag{2.1b}$$

In this formulation, σ is exponentially small as $\varepsilon \to 0$ for a metastable pattern with widely separated layers (cf. [20]).

An n-layer metastable pattern for (2.1), as shown in Fig. 1, is represented by the approximate form $u \sim u^*(x)$, where

$$u^*(x) = u^*(x; x_0, x_1, \ldots, x_{n-1}) \equiv u_s[\varepsilon^{-1}\xi_0(x - x_0)] + \sum_{j=1}^{n-1} \left(u_s[\varepsilon^{-1}\xi_j(x - x_j)] - s_j\right). \tag{2.2}$$

Here $u_s(z)$ is the unique heteroclinic orbit connecting s_- and s_+, which satisfies

$$u_s''(z) + Q\left[u_s(z)\right] = 0\,, \quad -\infty < z < \infty\,; \quad u_s(0) = 0\,; \;\; u_s'(z) = 0\,, \tag{2.3a}$$

and

$$u_s(z) \sim s_+ - a_+ e^{-\nu_+ z}\,, \;\; z \to +\infty\,; \quad u_s(z) \sim s_- + a_- e^{\nu_+ z}\,, \;\; z \to -\infty\,. \tag{2.3b}$$

The positive constants $\nu_\pm$ and $a_\pm$ in (2.3) are defined by

$$\nu_\pm = [-Q'(s_\pm)]^{\frac{1}{2}} \ , \quad \log a_\pm = \log(\pm s_\pm) + \int_0^{s_\pm} \left(\frac{\pm \nu_\pm}{[2V(\eta)]^{\frac{1}{2}}} + \frac{1}{\eta - s_\pm} \right) d\eta \, . \tag{2.4}$$

In (2.2), $x_j = x_j(t)$ for $j = 0, 1, \ldots, n-1$ are the unknown internal layer locations satisfying $x_{j-1}(t) < x_j(t)$. Since $u_s(0) = 0$, the curves $x = x_j(t)$, for $j = 0, 1, \ldots, n-1$, closely determine the locations of the zeros of $u(x,t)$ during the metastable evolution. The inter-layer distances $d_j = d_j(t)$ are given by $d_j = x_j - x_{j-1}$ for $j = 0, 1, \ldots, n$, where we have introduced the fictitious layers x_{-1} and x_n by $x_{-1} = -2 - x_0$ and $x_n = 2 - x_{n-1}$. These locations for x_{-1} and x_n correspond to the image points for x_0 and x_{n-1}, reflected through the endpoints $x = -1$ and $x = 1$, respectively. In the derivation of the ODE system for the $x_j(t)$, it is assumed that the layers are well-separated in the sense that $d_j(t) = O(1)$ as $\varepsilon \to 0$ for $j = 0, \ldots, n$. In (2.2) we have defined $\xi_j = (-1)^j \xi_0$, for $j = 0, \ldots, n-1$, where $\xi_0 = \pm 1$. This sequence specifies the orientation of each internal layer. In particular, in Fig. 1 we have $\xi_0 = 1$. Finally, in the formulae below, the triplet (a_j, ν_j, s_j) for $j = 0, \ldots, n$ is defined by

$$(a_j, \nu_j, s_j) = \begin{cases} (a_+, \nu_+, s_+) \, , & \text{when } \xi_j = -1 \, , \\ (a_-, \nu_-, s_-) \, , & \text{when } \xi_j = +1 \, . \end{cases} \tag{2.5}$$

We now outline the analysis in [20]. To derive an ODE system for the $x_j(t)$, we first introduce the quasi-steady linearization of (2.1). We substitute $u(x,t) = u^*(x) + w(x,t)$ into (2.1) under the assumption that $w \ll u^*$, $w_t \ll u^*_t$, and $\sigma \ll 1$, to obtain

$$\varepsilon^2 w_{xx} \ + \ Q'(u^*) w = \sigma + E(x) + \alpha \kappa u^*_t \, , \tag{2.6a}$$

$$w_x(-1,t) \ \sim \ -\varepsilon^{-1} \xi_0 a_0 \nu_0 e^{-\varepsilon^{-1} \nu_0 d_0} \, , \qquad w_x(1,t) \sim -\varepsilon^{-1} \xi_{n-1} a_n \nu_n e^{-\varepsilon^{-1} \nu_n d_n} \, , \tag{2.6b}$$

$$\sigma_{xx} \ = \ (1-\alpha) \varepsilon^{-1} \sum_{j=0}^{n-1} \xi_j \, \dot{x}_j \, u_s'[\varepsilon^{-1} \xi_j (x - x_j)] \, , \qquad \sigma_x(\pm 1, t) = 0 \, . \tag{2.6c}$$

Here $E(x) = E(x; \, x_0, .., x_{n-1})$ is defined by

$$E(x; \, x_0, .., x_{n-1}) \equiv \sum_{j=0}^{n-1} Q\left(u_s[\varepsilon^{-1} \xi_j (x - x_j)] \right) - Q(u^*) \, . \tag{2.7}$$

The solvability condition for (2.6c) is that the mass constraint $m = \int_{-1}^{1} u^*(x; x_0, .., x_{n-1}) \, dx$ holds. Under this condition we integrate (2.6c) to get

$$\sigma(x,t) = (1-\alpha) \sum_{j=0}^{n-1} \dot{x}_j \, M_j(x; \, x_j) + \sigma_c(t) \, , \tag{2.8a}$$

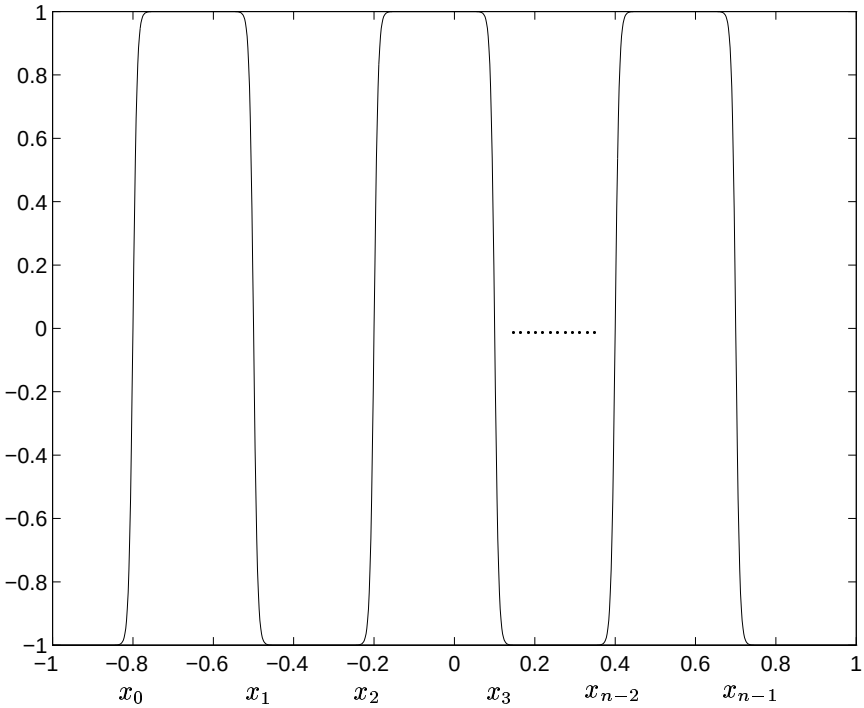

Figure 1: An n-layer metastable pattern for the viscous Cahn-Hilliard equation (2.1).

where $\sigma_c(t)$ is a function to be determined, and

$$M_j(x;\, x_j) \equiv \int_{-1}^{x} \left(u_s[\varepsilon^{-1}\xi_j(\eta - x_j)] - s_j \right)\, d\eta\,. \tag{2.8b}$$

The eigenvalue problem associated with (2.6a), (2.6b) is

$$\varepsilon^2\phi_{xx} + Q'(u^*)\,\phi \;=\; \lambda\,\phi\,, \quad -1 < x < 1\,; \qquad (\phi,\phi) = 1\,, \tag{2.9a}$$

$$\phi_x(-1) = 0\,, \qquad \phi_x(1) \;=\; 0\,, \tag{2.9b}$$

where $(u,v) \equiv \int_{-1}^{1} uv\,dx$. The first n eigenvalues λ_j for $j = 0,..,n-1$ are exponentially small as $\varepsilon \to 0$ (cf. [9]) and the corresponding normalized eigenfunctions are $\phi_j(x) \sim R_j u_s'[\varepsilon^{-1}\xi_j(x - x_j)]$, where R_j is a normalization constant. The eigenfunction expansion of w, found by integration by parts, is

$$w = \sum_{j=0}^{\infty} \frac{c_j\phi_j}{\lambda_j}\,, \qquad c_j \equiv (E,\phi_j) + (\sigma,\phi_j) + \alpha\kappa\,(u_t^*,\phi_j) - \varepsilon^2\phi_j w_x|_{-1}^{1}\,. \tag{2.10}$$

Since $\lambda_j \to 0$ exponentially as $\varepsilon \to 0$ we must impose the limiting solvability conditions that $c_j = 0$ for $j = 0, .., n-1$. This projection step yields the coupled system for $\sigma_c(t)$ and $x_j(t)$, for $j = 0, .., n-1$,

$$(1-\alpha)\sum_{k=0}^{n-1} \dot{x}_k \ (M_k, \phi_j) + (\sigma_c, \phi_j) + \alpha\kappa\,(u_t^*, \phi_j) \sim \varepsilon^2 \phi_j w_x|_{-1}^{1} - (E, \phi_j) \ , \tag{2.11}$$

which is to be solved together with the mass constraint $m = \int_{-1}^{1} u^*(x; x_0, .., x_{n-1})\, dx$.

Finally, the asymptotic form $\phi_j(x) \sim R_j u_s'[\varepsilon^{-1}\xi_j(x - x_j)]$ is used to evaluate the various terms in (2.11) for $\varepsilon \to 0$, with the following result:

Proposition 1 (From [20]): *For $\varepsilon \to 0$, an n-layer metastable pattern for (2.1) with widely separated layers is represented by (2.2), where $x_j(t)$ for $j = 0, 1, \ldots, n-1$, and $\sigma_c(t)$ in (2.8a) satisfy the explicit differential-algebraic (DAE) system*

$$\alpha\kappa\beta\varepsilon^{-1}\dot{x}_j + (1-\alpha)\sum_{k=0}^{n-1} \dot{x}_k b_{j,k} \quad \sim \quad \sigma_c \xi_j (s_+ - s_-) + H_j \,, \qquad j = 0, 1, \ldots, n-1 \,, \tag{2.12a}$$

$$\sum_{k=0}^{n} s_k (x_k - x_{k-1}) \quad \sim \quad m - \varepsilon n(\theta_- - \theta_+) \,. \tag{2.12b}$$

Here the exponentially weak forces H_j for $j = 0, 1, \ldots, n-1$ and the coupling coefficients $b_{j,k}$ for $j, k = 0, 1, \ldots, n-1$ are defined by

$$H_j \quad \equiv \quad 2\left(a_{j+1}^2 \nu_{j+1}^2 e^{-\varepsilon^{-1}\nu_{j+1} d_{j+1}} - a_j^2 \nu_j^2 e^{-\varepsilon^{-1}\nu_j d_j}\right) \,, \tag{2.13a}$$

$$b_{j,k} \quad \equiv \quad \int_{-1}^{1} \left(u_s[\varepsilon^{-1}\xi_k(x - x_k)] - s_k\right)\left(u_s[\varepsilon^{-1}\xi_j(x - x_j)] - s_{j+1}\right) dx \,, \tag{2.13b}$$

where

$$\beta \equiv \int_{-\infty}^{\infty} [u_s'(z)]^2 dz \,, \quad \theta_- \equiv \int_{-\infty}^{0} [u_s(\eta) - s_-]\, d\eta \,, \quad \theta_+ \equiv \int_{0}^{\infty} [s_+ - u_s(\eta)]\, d\eta \,. \tag{2.14}$$

The coefficients a_j, ν_j and s_j are defined in (2.5).

The asymptotic reduction of (2.12) and the qualitative features of the metastability and coarsening, which were not examined in [20], are studied in §3 and §4.

2.1 Numerical Treatment of the Viscous Cahn-Hilliard Equation

To validate the results from the asymptotic DAE system (2.12), we compared them with corresponding numerical results computed from the full problem (2.1) using a transverse method of lines (TMOL) (cf. [3]) approach. The specific TMOL we used was based on replacing the time derivative term u_t in (2.1) by a m-th order backward differentiation scheme (BDF) (cf. [10]). This converts (2.1) into a set of boundary

value problems for $u_n(x)$ and $\sigma_n(x)$, which represents the unknowns u and σ at each time step. These boundary value problems were then solved by using the boundary value problem solver COLSYS [2]. The solver COLSYS computes solutions using a collocation method and automatically interpolates and inserts mesh points where needed in order to satisfy a prescribed error tolerance. It also allows for a simple Euler continuation and so the solution at a previous time-step can be readily used as an initial guess for the next time step. Although this approach was computationally expensive, it yielded approximate solutions to (2.1) that are highly accurate in space. Since several time scales do occur, we found it necessary to implement a time-stepping control strategy to efficiently track the solution to (2.1) over long time intervals. To achive this, we employed a $(m+1)$-th order BDF scheme at each time step for the purpose of comparison, and used the l_2-norm of the difference between the solutions of the m-th and the $(m+1)$-th order BDF schemes as an error indicator to reject large inaccurate time steps or to enlarge unnecessarily small time steps. In all of the calculations below we took $m = 2$. This numerical procedure worked well for $0 \leq \alpha < 1$, but was modified when $\alpha = 1$.

d_3	t(num.)	t(asy.)
0.2499637	0.11805135 $\times 10^2$	0.11805099 $\times 10^2$
0.2490057	0.31421876 $\times 10^3$	0.31423049 $\times 10^3$
0.2457128	0.12120381 $\times 10^4$	0.12121263 $\times 10^4$
0.2353902	0.30076767 $\times 10^4$	0.30080758 $\times 10^4$
0.2221106	0.40610571 $\times 10^4$	0.40615483 $\times 10^4$
0.2049384	0.45628835 $\times 10^4$	0.45634494 $\times 10^4$
0.1503616	0.47902868 $\times 10^4$	0.47909376 $\times 10^4$
0.1028643	0.47961152 $\times 10^4$	0.47967273 $\times 10^4$
0.0697038	0.47963267 $\times 10^4$	0.47971114 $\times 10^4$

Table 1: A comparison of the asymptotic and numerical results for $t = t(d_3)$ for the Cahn-Hilliard equation ($\alpha = 0$) with $\varepsilon = 0.03$. The initial values of x_j for $j = 0, \ldots, 5$ were -0.70, -0.40, -0.10, 0.15, 0.50, 0.80.

When $\alpha = 1$ we computed solutions to the constrained Allen-Cahn equation (1.4) by first discretizing u_t in (1.4) by a second-order BDF scheme

$$\sum_{j=0}^{2} \beta_j u_{n-j}(x) = \beta_{n+1} \left(\varepsilon^2 (u_n)_{xx} + Q(u_n) - \frac{1}{2} \int_{-1}^{1} Q(u_n) dx \right) , \quad (u_n)_x(\pm 1) = 0 , \tag{2.15}$$

where β_j are the coefficients of the BDF scheme. Since the resulting boundary value problems are nonlocal in space, COLSYS cannot immediately be used. To circumvent this difficulty, we introduced the new variables

d_3	t(num.)	t(asy.)
0.2499080	0.10960657×10^2	0.10947517×10^2
0.2457898	0.45001770×10^3	0.45013814×10^3
0.2354383	0.11982005×10^4	0.11986815×10^4
0.2268495	0.15722918×10^4	0.15731235×10^4
0.2068120	0.20064226×10^4	0.20078002×10^4
0.1687788	0.22184970×10^4	0.22204742×10^4
0.1484624	0.22420676×10^4	0.22442599×10^4
0.1016572	0.22539916×10^4	0.22564691×10^4
0.0545736	0.22551925×10^4	0.22576482×10^4

Table 2: A comparison of the asymptotic and numerical results for $t = t(d_3)$ for the viscous Cahn-Hilliard equation ($\alpha = 0.5$) with $\varepsilon = 0.04$. The initial values of x_j for $j = 0, \ldots, 5$ were -0.70, -0.40, -0.10, 0.15, 0.50, 0.80.

$\boldsymbol{z} = (z_1, \ldots, z_4)^T$, where

$$z_1 = u_n\,, \quad z_2 = (u_n)_x\,, \quad z_3 = \int_{-1}^{1} Q(u_n)dx\,, \quad z_4 = \int_{-1}^{x} Q(u_n)dx \Big/ \int_{-1}^{1} Q(u_n)dx\,. \tag{2.16}$$

With these new variables, (2.15) is reduced to the local problem

$$\boldsymbol{z}_x = F(\boldsymbol{z})\,, \qquad z_2(-1) = z_2(1) = z_4(-1) = 0\,, \quad z_4(1) = 1\,, \tag{2.17}$$

where the nonlinear function $F : R^4 \to R^4$ can be easily derived from (2.15) and (2.16). Then, COLSYS was used to solve the boundary value problem (2.17) at each time step.

In all of the comparisons below between the asymptotic and numerical results for σ_c and for the internal layer locations x_j, we took $Q(u) = 2(u - u^3)$ and $\kappa = 1$. For this form of $Q(u)$, the heteroclinic orbit constants needed in (2.12) and (2.13) are given analytically by

$$a_\pm = 2\,, \quad \nu_\pm = 2\,, \quad s_\pm = \pm 1\,, \quad \beta = 4/3\,, \quad \theta_\pm = \log 2\,. \tag{2.18}$$

In the comparisons below, we chose different values of α corresponding to the different types of phase separation models and we took $u(x,0) = u^*(x; x_0^0, \ldots, x_{n-1}^0)$ as the initial data for (2.1). Here u^* is the n-layer metastable pattern (2.2) and $x_j^0 \in (-1,\, 1)\,, j = 0, 1, \ldots, n-1$ are the initial zeros of u. To eliminate any unwanted transient effects, we computed the full numerical solution to (2.1) with this initial data until $t = t_c$, where t_c was some $O(1)$ positive constant. We then reset x_j^0, for $j = 0, \ldots, n-1$, to be the zeros of the numerical approximation u^h at time $t = t_c$. With these new values of x_j^0 as its initial data, the

d_3	t(num.)	t(asy.)
0.2499500	0.11561895×10^2	0.11528481×10^2
0.2494742	0.12103537×10^3	0.12102348×10^3
0.2450228	0.10128793×10^4	0.10130617×10^4
0.2370225	0.21550525×10^4	0.21555446×10^4
0.2201322	0.34372605×10^4	0.34383206×10^4
0.2058314	0.39218631×10^4	0.39233456×10^4
0.1635920	0.43265906×10^4	0.43291128×10^4
0.1171353	0.43761505×10^4	0.43793961×10^4
0.0497620	0.43813902×10^4	0.43846704×10^4

Table 3: A comparison of the asymptotic and numerical results for $t = t(d_3)$ for the constrained Allen-Cahn equation ($\alpha = 1$) with $\varepsilon = 0.04$. The initial values of x_j for $j = 0, \ldots, 5$ were -0.70, -0.40, -0.10, 0.15, 0.50, 0.80.

DAE system (2.12) was solved numerically using the implicit ODE-solver LSODI (cf. [15]) and results were compared with corresponding full numerical results.

It has been clear from [6] and [20] that the internal layers that are initially closest together will move towards each other at an extremely slow rate and eventually undergo a collapse phase, leaving behind a metastable pattern with two fewer layers. In Tables 1 – 3, we give a comparison between the asymptotic and numerical results for the evolution of these collapse layers for three types of phase separation models corresponding to $\alpha = 0$, $\frac{1}{2}$ and 1. In these tables, the initial values of x_j for $j = 0, \ldots, n-1$ with $n = 6$ were chosen to be near -0.7, -0.4, -0.1, 0.15, 0.5 and 0.8. For this data d_3 will approach zero as t increases. The second and third columns in Tables 1 – 3 compare the numerical and asymptotic elapsed time t necessary for the distance d_3 to be given by the values in the first column. These elapsed times are found to agree to more than three significant digits. In Fig. 2 – 4, we plot the full numerical solutions at different times to (2.1) corresponding to the parameter values used for Table 1 – 3, respectively. The behavior of the solution during the metastable phase and the collapse phase shown in these figures will be discussed in the next few sections.

3 An Asymptotic Reduction for the Metastable Dynamics

The DAE system (2.12) provides a quantitative characterization of metastable internal layer motion for the viscous Cahn-Hilliard equation (2.1). However, it is not easily analyzed and thus gives little direct analytical information. In this section, we asymptotically decouple (2.12) for $\varepsilon \ll 1$ and then study the corresponding

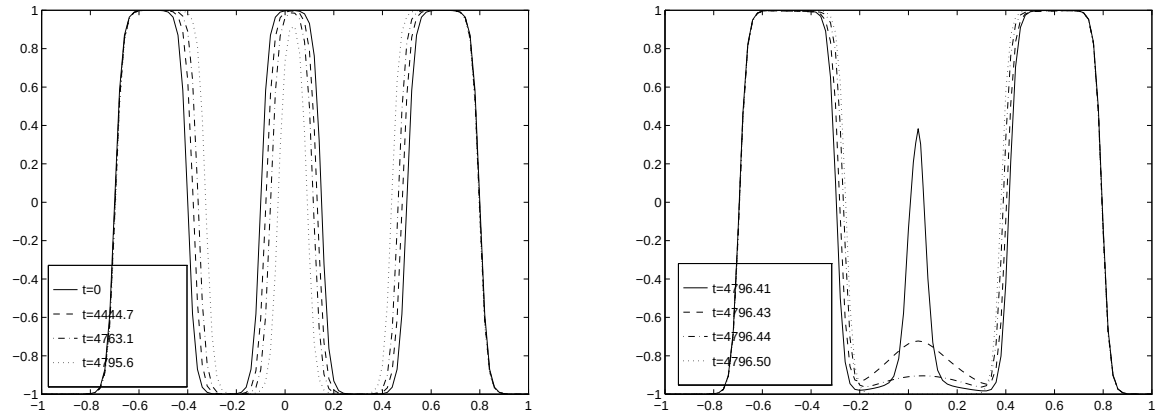

Figure 2: Plot of the numerical solution to the Cahn-Hilliard equation ($\alpha = 0$) at different times corresponding to the parameter values given in Table 1.

reduced system to reveal the analytical behavior of the metastable dynamics associated with the different phase separation models. In the analysis below, there will be two ranges of α that need to be distinguished: $0 < \alpha \leq 1$ (referred to as the viscous case) and $\alpha = 0$ (the Cahn-Hilliard equation). Since the dynamics of two internal layers ($n = 2$) was studied in [20], we will focus below only on the case where $n > 2$. Numerical results are provided to illustrate our analysis.

3.1 The Viscous Case: Asymptotic Reduction

We first decouple (2.12) for the viscous parameter range $0 < \alpha \leq 1$. In [20], the coefficients $b_{j,k}$ defined in (2.13b) were evaluated asymptotically to within negligible exponentially small terms as

$$b_{j,k} \sim -(-1)^{j+k}(x_j - x_k)(s_+ - s_-)^2 - \varepsilon\left[1 - (-1)^{j+k}\right]\xi_j(s_+ - s_-)(\theta_- - \theta_+)\,, \quad \text{for } j > k\,, \tag{3.1a}$$

$$b_{j,j} \sim -\varepsilon\mu\,; \quad b_{j,k} = O(e^{-\varepsilon^{-1}c})\,, \quad \text{for } j < k\,. \tag{3.1b}$$

Here μ is defined by

$$\mu \equiv \int_{-\infty}^{\infty} [s_+ - u_s(\eta)][u_s(\eta) - s_-]d\eta\,, \tag{3.2}$$

and c is a positive constant that is proportional to the distance $|x_k - x_j|$.

Next, using (3.1), we can rewrite (2.12a) in matrix form as

$$\alpha\kappa\beta\varepsilon^{-1}\dot{\mathbf{x}} + (1-\alpha)\left(B_0 + \varepsilon B_1\right)\dot{\mathbf{x}} \sim \sigma_c(s_+ - s_-)\xi + \mathbf{H}\,, \tag{3.3a}$$

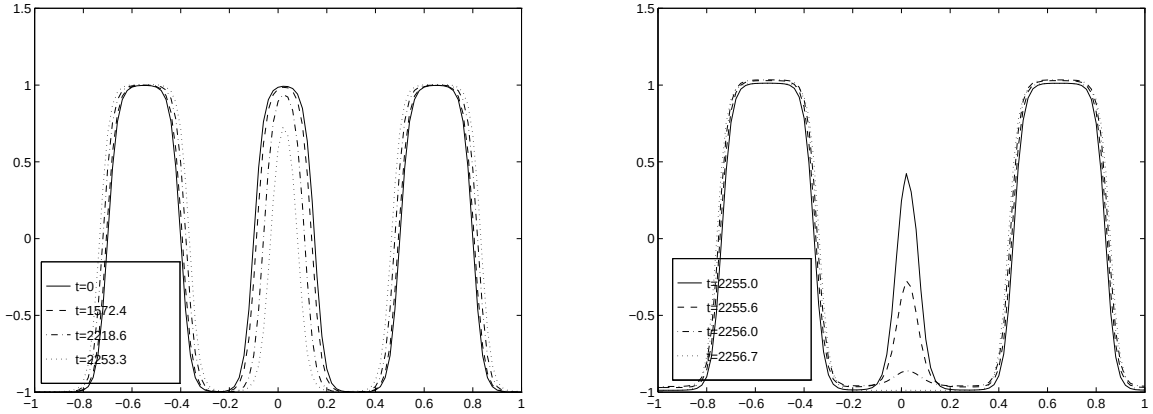

Figure 3: Plot of the numerical solution to the viscous Cahn-Hilliard equation ($\alpha = 1/2$) at different times corresponding to the parameter values given in Table 2.

where the entries $b^{(0)}_{j,k}$ and $b^{(1)}_{j,k}$ of the matrices B_0 and B_1 are given by

$$b^{(0)}_{j,k} = 0\,,\ \ j \le k\,; \quad b^{(0)}_{j,k} = -(-1)^{j+k}(x_j - x_k)(s_+ - s_-)^2\,,\ \ j > k\,, \tag{3.3b}$$

$$b^{(1)}_{j,k} = 0\,,\ \ j < k\,; \quad b^{(1)}_{j,j} = -\mu\,; \quad b^{(1)}_{j,k} = -\left[1 - (-1)^{j+k}\right]\xi_j(s_+ - s_-)(\theta_- - \theta_+)\,,\ \ j > k\,. \tag{3.3c}$$

Here we have defined

$$\dot{\mathbf{x}} \equiv \begin{pmatrix} \dot{x}_0 \\ \vdots \\ \dot{x}_{n-1} \end{pmatrix}\,, \quad \xi \equiv \begin{pmatrix} \xi_0 \\ \vdots \\ \xi_{n-1} \end{pmatrix}\,, \quad \mathbf{H} \equiv \begin{pmatrix} H_0 \\ \vdots \\ H_{n-1} \end{pmatrix}\,. \tag{3.3d}$$

Next, by differentiating (2.12b) with respect to t, we find that the mass constraint is equivalent to the dot product

$$\xi \cdot \dot{\mathbf{x}} = 0\,. \tag{3.4}$$

The following asymptotic reduction of (2.12) is then obtained by substituting an asymptotic expansion of $\dot{\mathbf{x}}$ and σ_c in powers of ε into (3.3a) and (3.4):

Corollary 1: *Consider the viscous case where $0 < \alpha \le 1$. Then, for $\varepsilon \to 0$, an n-layer metastable pattern for (2.1) with widely separated layers is represented by (2.2), where σ_c and the vector $\mathbf{x}$, representing the unknown internal layer locations, satisfy the ODE system*

$$\dot{\mathbf{x}} \sim \varepsilon\dot{\mathbf{x}}^{(0)} + \varepsilon^2\dot{\mathbf{x}}^{(1)} + \cdots\,, \quad \sigma_c \sim \sigma_c^{(0)} + \varepsilon\sigma_c^{(1)} + \cdots\,, \tag{3.5a}$$

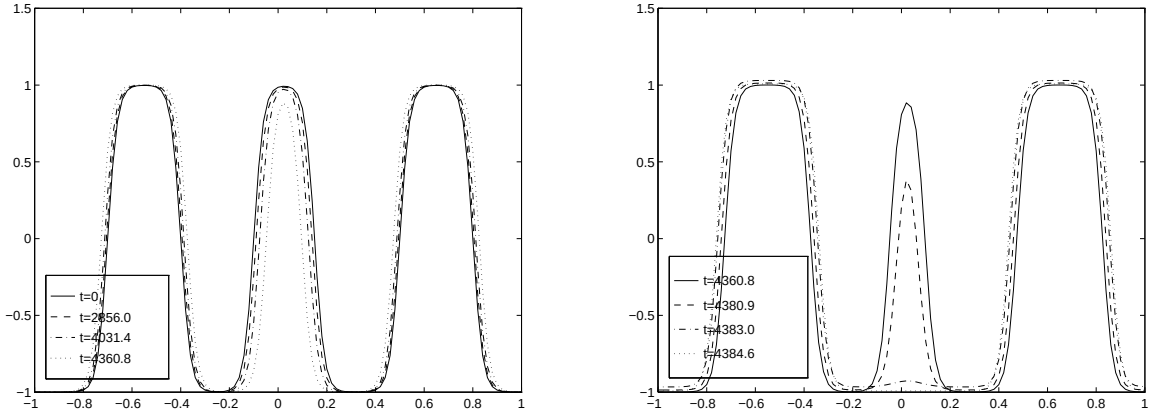

Figure 4: Plot of the numerical solution to the constrained Allen-Cahn equation ($\alpha = 1$) at different times corresponding to the parameter values given in Table 3.

where

$$\dot{\mathbf{x}}^{(0)} = \frac{1}{\alpha\kappa\beta}\left[\mathbf{H} - \frac{1}{n}\left(\xi\cdot\mathbf{H}\right)\xi\right], \qquad \sigma_c^{(0)} = -\frac{1}{n(s_+ - s_-)}\xi\cdot\mathbf{H}, \tag{3.5b}$$

$$\dot{\mathbf{x}}^{(1)} = -\frac{(1-\alpha)}{\alpha\kappa\beta}\left[B_0\dot{\mathbf{x}}^{(0)} + \frac{1}{n}\left[\xi\cdot\left(B_0\dot{\mathbf{x}}^{(0)}\right)\right]\xi\right], \qquad \sigma_c^{(1)} = -\frac{(1-\alpha)}{n(s_+ - s_-)}\xi\cdot\left(B_0\dot{\mathbf{x}}^{(0)}\right). \tag{3.5c}$$

This result has two interesting implications. Firstly, for the constrained Allen-Cahn equation where $\alpha = 1$, we have $\dot{\mathbf{x}} = \varepsilon\dot{\mathbf{x}}^{(0)}$ and $\sigma_c = \sigma_c^{(0)}$, since the higher order terms in (3.5) vanish. Secondly, we observe that, up to terms of $O(\varepsilon)$, the metastable dynamics associated with the viscous Cahn-Hilliard equation ($0 < \alpha < 1$) are exactly the same as those associated with the constrained Allen-Cahn equation ($\alpha = 1$), except for the minor difference of a multiplicative factor of α in the time scale.

3.2 The Cahn-Hilliard Equation: Asymptotic Reduction

Next, we asymptotically reduce (2.12) for the more intricate case of the Cahn-Hilliard equation where $\alpha = 0$. In this case, it is convenient to add up two consecutive ODE's in (2.12a) to get $n-1$ equations for the unknowns x_0, x_1,..,x_{n-1}. Since $\xi_j = -\xi_{j+1}$, this procedure eliminates σ_c from the system and yields

$$\dot{x}_0\left(b_{j,0} + b_{j+1,0}\right) + \cdots + \dot{x}_j\left(b_{j,j} + b_{j+1,j}\right) + \dot{x}_{j+1}b_{j+1,j+1} \sim H_{j+1} + H_j\,, \tag{3.6}$$

for $j = 0, \ldots, n-2$. Now using (3.1) we can calculate the coefficients in (3.6) as

$$b_{j,k} + b_{j+1,k} \sim \zeta_j (-1)^{j+k}, \qquad 0 \le k < j, \tag{3.7a}$$

$$b_{j,j} + b_{j+1,j} \sim \zeta_j - \varepsilon\mu, \qquad j \ge 0, \tag{3.7b}$$

$$b_{j,j} \sim -\varepsilon\mu. \tag{3.7c}$$

Here we have defined ζ_j by

$$\zeta_j \equiv (x_{j+1} - x_j)(s_+ - s_-)^2 + 2\varepsilon\xi_j(s_+ - s_-)(\theta_- - \theta_+), \tag{3.7d}$$

where $\theta_\pm$ were defined in (2.14).

Combining (3.6) together with the relation $\sum_{j=0}^{n-1}(-1)^j \dot{x}_j = 0$ derived from the mass constraint, we can readily write the system for the $\dot{x}_j$ in matrix form as

$$(A - \varepsilon U)\,\dot{\mathbf{x}} \sim \mathbf{r}, \tag{3.8a}$$

where the $n \times n$ matrices A and U, and the n-vectors $\dot{\mathbf{x}}$ and $\mathbf{r}$ are defined by

$$A \equiv \begin{pmatrix} 1 & 0 & 0 & 0 & \ldots & 0 & 0 \\ -1 & 1 & 0 & 0 & \ldots & 0 & 0 \\ 1 & -1 & 1 & 0 & \ldots & 0 & 0 \\ \vdots & \vdots & \vdots & \vdots & & \vdots & \vdots \\ (-1)^{n-1} & -(-1)^{n-1} & (-1)^{n-1} & -(-1)^{n-1} & \ldots & -1 & 1 \end{pmatrix}, \qquad \dot{\mathbf{x}} \equiv \begin{pmatrix} \dot{x}_0 \\ \vdots \\ \dot{x}_{n-1} \end{pmatrix}, \tag{3.8b}$$

$$U \equiv \begin{pmatrix} \mu_0 & \mu_0 & 0 & 0 & \ldots & 0 & 0 \\ 0 & \mu_1 & \mu_1 & 0 & \ldots & 0 & 0 \\ 0 & 0 & \mu_2 & \mu_2 & \ldots & 0 & 0 \\ \vdots & \vdots & \vdots & \vdots & & \vdots & \vdots \\ 0 & 0 & 0 & 0 & \ldots & \mu_{n-2} & \mu_{n-2} \\ 0 & 0 & 0 & 0 & \ldots & 0 & 0 \end{pmatrix}, \qquad \mathbf{r} \equiv \begin{pmatrix} r_0 \\ r_1 \\ \vdots \\ r_{n-2} \\ 0 \end{pmatrix}. \tag{3.8c}$$

Here, for $0 \le j \le n-2$, we have defined μ_j and r_j by

$$\mu_j \equiv \mu\zeta_j^{-1}, \tag{3.8d}$$

$$r_j \equiv \zeta_j^{-1}(H_j + H_{j+1}) = 2\zeta_j^{-1}\left(a_{j+2}^2\nu_{j+2}^2 e^{-\varepsilon^{-1}\nu_{j+2}d_{j+2}} - a_j^2\nu_j^2 e^{-\varepsilon^{-1}\nu_j d_j}\right). \tag{3.8e}$$

The coefficients ν_j, a_j are defined in (2.5), μ is defined in (3.2), ζ_j is defined in (3.7d), and $d_j = x_j - x_{j-1}$.

To obtain an explicit set of ODE's for the x_j we must calculate the inverse matrix $(A - \varepsilon U)^{-1}$. Since this cannot easily be done in closed form, we instead expand

$$\dot{\mathbf{x}} \sim \dot{\mathbf{x}}^{(0)} + \sum_{k=1}^{\infty} \varepsilon^k \dot{\mathbf{x}}^{(k)}, \tag{3.9}$$

for some unknowns $\dot{\mathbf{x}}^{(k)}$. In this way, in the formulae below we need only the explicit inverse

$$A^{-1} \equiv \begin{pmatrix} 1 & 0 & 0 & 0 & \dots & 0 & 0 \\ 1 & 1 & 0 & 0 & \dots & 0 & 0 \\ 0 & 1 & 1 & 0 & \dots & 0 & 0 \\ 0 & 0 & 1 & 1 & \dots & 0 & 0 \\ \vdots & \vdots & \vdots & \vdots & & \vdots & \vdots \\ 0 & 0 & 0 & 0 & \dots & 1 & 1 \end{pmatrix} . \tag{3.10}$$

Substituting (3.9) into (3.8a) and collecting powers of ε we obtain an explicit ODE system. Then, the function $\sigma_c(t)$ is conveniently evaluated from (2.12a) when $j = 0$ and $\alpha = 0$. We summarize the result as follows:

Corollary 2: *Consider the Cahn-Hilliard equation where $\alpha = 0$. Then, for $\varepsilon \to 0$, an n-layer metastable pattern for (2.1) with widely separated layers is represented by (2.2), where σ_c and the vector $\mathbf{x}$, representing the unknown internal layer locations, satisfy the ODE system*

$$\dot{\mathbf{x}} \sim \dot{\mathbf{x}}^{(0)} + \varepsilon(A^{-1}U)\dot{\mathbf{x}}^{(0)} + \sum_{k=2}^{\infty} \varepsilon^k (A^{-1}U)^k \dot{\mathbf{x}}^{(0)} . \tag{3.11a}$$

$$\sigma_c \sim -\frac{(H_0 + \varepsilon\mu\dot{x}_0)}{\xi_0(s_+ - s_-)} . \tag{3.11b}$$

Here

$$A^{-1}U \equiv \begin{pmatrix} \mu_0 & \mu_0 & 0 & 0 & \dots & 0 & 0 & 0 \\ \mu_0 & \mu_0 + \mu_1 & \mu_1 & 0 & \dots & 0 & 0 & 0 \\ 0 & \mu_1 & \mu_1 + \mu_2 & \mu_2 & \dots & 0 & 0 & 0 \\ \vdots & \vdots & \vdots & \vdots & & \vdots & \vdots & \vdots \\ 0 & 0 & 0 & 0 & \dots & \mu_{n-3} & \mu_{n-3} + \mu_{n-2} & \mu_{n-2} \\ 0 & 0 & 0 & 0 & \dots & 0 & \mu_{n-2} & \mu_{n-2} \end{pmatrix} , \quad \dot{\mathbf{x}}^{(0)} \equiv \begin{pmatrix} r_0 \\ r_0 + r_1 \\ r_1 + r_2 \\ \vdots \\ r_{n-3} + r_{n-2} \\ r_{n-2} \end{pmatrix} . \tag{3.11c}$$

In (3.11b), $\dot{x}_0$ is the first element of $\dot{\mathbf{x}}$. Also, μ_j and r_j are defined in (3.8d) and (3.8e), respectively.

As a partial check on our results, we calculated numerical values for the asymptotic estimates for σ_c in (3.5a) and (3.11b) for various sets of internal layer locations. The results were found to compare very favorably with corresponding numerical results computed directly from (2.12) using the software package LSODI (cf. [15]). These comparisons are shown in Tables 4 and 5 for the Cahn-Hilliard and the viscous Cahn-Hilliard equation with $\alpha = 1/2$, respectively.

(x_0, x_1, x_2, x_3)	σ_c (num.)	σ_c (3.11b)
$(-0.9, -0.4, 0, 0.6)$	0.336661×10^{-7}	0.336380×10^{-7}
$(-0.4, -0.1, 0.1, 0.5)$	-0.117992×10^{-8}	-0.109940×10^{-8}
$(-0.5, -0.2, 0.2, 0.8)$	$-0.149581 \times 10^{-11}$	$-0.149597 \times 10^{-11}$
$(-0.6, -0.2, 0.2, 0.6)$	$-0.697625 \times 10^{-16}$	$-0.696720 \times 10^{-16}$
$(-0.7, -0.3, 0.25, 0.6)$	$-0.729543 \times 10^{-16}$	$-0.725283 \times 10^{-16}$

Table 4: A comparison of the asymptotic and numerical results for σ_c for the Cahn-Hilliard equation ($\alpha = 0$) with $\varepsilon = 0.02$.

(x_0, x_1, x_2, x_3)	σ_c (num.)	σ_c (3.5a)
$(-0.5, -0.1, 0.1, 0.5)$	0.127273×10^{-4}	0.129567×10^{-4}
$(-0.7, -0.3, 0, 0.5)$	0.162085×10^{-7}	0.164682×10^{-7}
$(-0.5, -0.1, 0.3, 0.7)$	$-0.213520 \times 10^{-10}$	$-0.209847 \times 10^{-10}$
$(-0.75, -0.25, 0.2, 0.75)$	0.738668×10^{-12}	0.747657×10^{-12}

Table 5: A comparison of the asymptotic and numerical results for σ_c for the viscous Cahn-Hilliard equation ($\alpha = \frac{1}{2}$) with $\varepsilon = 0.03$.

4 Metastable Dynamics and Layer Collapse Events

In this section we analyze the behavior of the solution to our ODE systems (3.5) and (3.11) during a layer collapse event. We assume that the initial data $x_j(0)$ is given. Since, H_j in (2.13a) depends exponentially on ε, the interval which collapses first is the one for which $\nu_j d_j$ is smallest at $t = 0$. Assume that this occurs for $j = J$, so that the interval (x_{J-1}, x_J) is annihilated first. The ODE systems (3.5) and (3.11), are then asymptotically dominated by differential equations for x_{J-1} and x_J. The primary goal is to derive a differential equation for $d_J = x_J - x_{J-1}$ and to determine the behavior of the remaining layers as d_J collapses to zero. This analysis is needed in §5 in order to devise an algorithm to simulate the entire coarsening process. The analysis also reveals that at the onset of a collapse event the behavior of the solution for the viscous case is very different than for the Cahn-Hilliard model. To supplement the analysis, in Figs. 5–7 we have plotted numerical results to illustrate various types of layer collapse events for the three phase separation models corresponding to $\alpha = 0$, $\alpha = 1/2$, and $\alpha = 1$. These results are computed from (2.1) using the TMOL method. Another goal is to explain the observable featues in these plots. In Fig. 5 we plot a collapse event when the internal layers are away from the endpoints. In Fig. 6 we plot the collapse of an internal layer against the endpoint $x = 1$. Finally, in Fig. 7 we plot solutions when there are a pair of collapsing

intervals. In this section it is convenient to introduce the notation $f = o'(g)$, by which we mean that f is exponentially small than g as $\varepsilon \to 0$.

4.1 The Viscous Case: The Collapse of One Interval

Let $n \geq 3$ and label $d_j(0)$ for $j = 0, \ldots, n$ by $d_j^0 = d_j(0)$. Assume that there is a J with $1 \leq J \leq n-1$ such that $\nu_J d_J^0 < \nu_j d_j^0$ for all $j = 0, \ldots, n$ with $j \neq J$. Thus, for $\varepsilon \ll 1$, the pair of internal layers x_{J-1} and x_J will collapse first. Then, from (2.13a) we have $H_J \sim -H_{J-1} \sim -2a_J^2\nu_J^2 e^{-\varepsilon^{-1}\nu_J d_J}$, and $H_j = o'(H_J)$ for all $j = 0, \ldots, n$ with $j \neq J$ and $j \neq J-1$. Then, from the leading $O(\varepsilon)$ term in (3.5a) we get

$$\dot{x}_{J-1} \sim \frac{\varepsilon}{\alpha\kappa\beta} H_{J-1}\left(1 - \frac{2}{n}\right), \qquad \dot{x}_J \sim -\frac{\varepsilon}{\alpha\kappa\beta} H_{J-1}\left(1 - \frac{2}{n}\right). \tag{4.1}$$

Therefore, $d_J = x_J - x_{J-1}$ satisfies the ODE

$$\dot{d}_J \sim -\frac{4\varepsilon}{\alpha\kappa\beta}\left(1 - \frac{2}{n}\right) a_J^2\nu_J^2 e^{-\varepsilon^{-1}\nu_J d_J}, \qquad d_J(0) = d_J^0 > 0. \tag{4.2}$$

The solution is

$$d_J(t) \sim d_J^0 + \frac{\varepsilon}{\nu_J}\log[1 - t/t_s], \qquad t_s \equiv \frac{\alpha\kappa\beta[1-2/n]^{-1}}{4a_J^2\nu_J^3} e^{\varepsilon^{-1}\nu_J d_J^0}. \tag{4.3}$$

The layers x_{J-1} and x_J will collapse when $d_J(t) = 0$, which yields $t = t_s + O(1)$. It is interesting to note that the time for collapse depends on the number of layers initially present.

Now we explain the qualitative features in Fig. 3 and Fig. 4 by studying what happens to the remaining layers when d_J is collapsing to zero. From the $O(\varepsilon)$ term in (3.5a) we obtain

$$\dot{x}_{J-i} \sim \frac{2\varepsilon}{\alpha\kappa\beta n}(-1)^i H_{J-1}, \qquad 2 \leq i \leq J; \tag{4.4a}$$

$$\dot{x}_{J+i} \sim \frac{2\varepsilon}{\alpha\kappa\beta n}(-1)^i H_{J-1}, \qquad 1 \leq i \leq n-1-J. \tag{4.4b}$$

Therefore, as d_J is collapsing the other layers move asymptotically at a common speed but in alternate left and right directions. In other words, the mass of the disappearing interval will be consumed *evenly* by the other intervals as their widths expand. This is confirmed by the numerical results shown in Fig. 3 and Fig. 4 for $\alpha = 1/2$ and $\alpha = 1$, respectively. It is also confirmed in Figs. 5(c)–(f).

Now we consider the case when a layer first collapses against one of the endpoints. Thus, let $n \geq 2$ and assume that for $J = 0$ or $J = n$ that we have $\nu_J d_J^0 < \nu_j d_j^0$ for all $j = 0, \ldots, n$ and $j \neq J$. We will consider only the case when $J = n$. The case when $J = 0$ is similar. When $J = n$, we have from (2.13a) that $H_{n-1} \sim 2a_n^2\nu_n^2\, e^{-\varepsilon^{-1}\nu_n d_n}$ and that $H_j = o'(H_{n-1})$ for all $j = 0, \ldots, n$ with $j \neq n-1$. Then, from the

leading $O(\varepsilon)$ term in (3.5a) we get

$$\dot{x}_{n-1} \sim \frac{\varepsilon}{\alpha\kappa\beta} H_{n-1} \left(1 - \frac{1}{n}\right) ; \qquad \dot{x}_j \sim \frac{\varepsilon}{\alpha\kappa\beta n} (-1)^{n-j} H_{n-1} , \qquad \text{for } 0 \le j \le n-2 . \tag{4.5}$$

This means that as x_{n-1} is collapsing against the boundary at $x = 1$, the other layers will move at a common speed but in alternating directions. As a result, the change in mass due to the annihilation of x_{n-1} will be compensated by the remaining layers evenly. This is verified in Figs. 6(c)–(f), where we show numerical results of a layer collapsing against the endpoint $x = 1$. To solve for $x_{n-1}(t)$, we use $d_n = 2(1 - x_{n-1})$ to get from (4.5) that

$$\dot{x}_{n-1} \sim \frac{2\varepsilon}{\alpha\kappa\beta} \left(1 - \frac{1}{n}\right) a_n^2 \nu_n^2 e^{-2\varepsilon^{-1}\nu_n (1 - x_{n-1})} . \tag{4.6}$$

The solution to this ODE, with initial data $x_{n-1}^0 = x_{n-1}(0)$, is

$$x_{n-1}(t) \sim x_{n-1}(0) - \frac{\varepsilon}{2\nu_n} \log\left(1 - t/t_s\right) , \qquad t_s \equiv \frac{\alpha\kappa\beta[1 - 1/n]^{-1}}{4 a_n^2 \nu_n^3} \, e^{2\varepsilon^{-1}\nu_n (1 - x_{n-1}^0)} . \tag{4.7}$$

The dynamics is similar when $J = 0$.

4.2 The Cahn-Hilliard Equation: The Collapse of One Interval

Let $n \ge 4$ and label $d_j(0) = d_j^0$ for $j = 0, \ldots, n$. Assume that there is a J with $2 \le J \le n-2$ such that $\nu_J d_J^0 < \nu_j d_j^0$ for all $j = 0, \ldots, n$ with $j \ne J$. Thus, the pair of internal layers x_{J-1} and x_J will collapse first. Then, from (3.8e) and (3.7d), we calculate that

$$r_{J-2} \sim \frac{2}{d_{J-1}(s_+ - s_-)^2} a_J^2 \nu_J^2 e^{-\varepsilon^{-1}\nu_J d_J} , \qquad r_J \sim -\frac{2}{d_{J+1}(s_+ - s_-)^2} a_J^2 \nu_J^2 e^{-\varepsilon^{-1}\nu_J d_J} , \tag{4.8}$$

and $r_j = o'(r_J)$ for all $j = 0, \ldots, n$ with $j \ne J$ and $j \ne J-2$. Now from the leading terms in (3.11a) we get

$$\dot{x}_{J-2} \sim r_{J-2} > 0 ; \quad \dot{x}_{J-1} \sim r_{J-2} > 0 ; \quad \dot{x}_J \sim r_J < 0 ; \quad \dot{x}_{J+1} \sim r_J < 0 . \tag{4.9}$$

This means that the interfaces of the collapsing interval will approach each other and eventually coalesce, while the nearest neighboring interfaces move together in an asymptotically rigid way such that d_{J-1} and d_{J+1} remain asymptotically constant in time. This feature is clearly shown in Fig. 2. Hence $d_J = x_J - x_{J-1}$ satisfies the approximate ODE

$$d_J' \sim -\frac{2}{(s_+ - s_-)^2} a_J^2 \nu_J^2 e^{-\varepsilon^{-1}\nu_J d_J} \left(\frac{d_{J-1}^0 + d_{J+1}^0}{d_{J-1}^0 d_{J+1}^0}\right) , \qquad d_J(0) = d_J^0 > 0 , \tag{4.10}$$

where $d_{J-1}^0 = d_{J-1}(0)$ and $d_{J+1}^0 = d_{J+1}(0)$. The solution to (4.10) is

$$d_J(t) \sim d_J^0 + \frac{\varepsilon}{\nu_J} \log\left(1 - t/t_s\right) , \quad t_s \equiv \frac{\varepsilon (s_+ - s_-)^2}{2 a_J^2 \nu_J^3} \left(\frac{d_{J+1}^0 d_{J-1}^0}{d_{J+1}^0 + d_{J-1}^0}\right) e^{\varepsilon^{-1}\nu_J d_J^0} . \tag{4.11}$$

Notice that the time scale t_s for the collapse of $d_J(t)$ is very different from the corresponding result (4.3) for the viscous case. As $d_J(t)$ is tending to zero, we find from (3.11a) that the motion of the layers that are to the left of x_{J-2} and to the right of x_{J+1} satisfies

$$\dot{x}_{J-k} \sim \varepsilon^{k-2} r_{J-2}\omega_{-k}\,, \qquad k \geq 2\,; \qquad \dot{x}_{J+k} \sim -\varepsilon^{k-1} r_{J-2}\omega_k\,, \qquad k \geq 1\,. \tag{4.12}$$

Here $\omega_k > 0$ are $O(1)$ coefficients that can be found explicitly. This result follows from (3.11a) since $\left(A^{-1}U\right)^k$ is a matrix with bandwidth $2k+1$. Therefore, the layers x_{J-1} and x_{J-2} (x_J and x_{J+1}) will move at the same speed and direction to the right (left), and the other layers on the left (right) will move in the same direction as x_{J-1} and x_{J-2} (x_J and x_{J+1}), but at a successively slower speed, i.e., x_{J-k_1} with $k_1 \geq 3$ is $O(\varepsilon)$ slower than its right neighbor x_{J-k_1+1}. This conclusion is qualitatively seen in Fig. 2.

Now we analyze the behavior of (3.11) when the collapse layer is close to one of the endpoints. Let $n \geq 3$ and assume that for $J = 0, 1, n-1$ or n, we have $\nu_J d_J^0 < \nu_j d_j^0$ for all $j = 0, \ldots, n$ and $j \neq J$. If $J = n-1$, we then obtain from (3.8e) and (3.7d) that

$$r_{n-3} \sim \frac{2}{d_{n-2}(s_+ - s_-)^2} a_{n-1}^2 \nu_{n-1}^2 e^{-\varepsilon^{-1}\nu_{n-1}d_{n-1}}\,, \tag{4.13}$$

and $r_j = o'(r_{n-3})$ for all $j = 0, \ldots, n$ with $j \neq n-3$. Thus, we obtain from (3.11a) that

$$\dot{x}_{n-3} \sim r_{n-3}\,; \quad \dot{x}_{n-2} \sim r_{n-3}\,; \quad \dot{x}_{n-1} \sim \varepsilon\mu_{n-2} r_{n-3}\,; \quad \dot{x}_j \sim \varepsilon^{n-3-j} r_{n-3}\omega_j\,, \qquad 0 \leq j \leq n-4\,. \tag{4.14}$$

Thus, although all of the layers move to the right, their speeds are different. The layers x_{n-3} and x_{n-2} are moving at the same speed r_{n-3}, while the other layers are essentially static. This is verified in Figs. 5(a), (b). Since, to within $O(\varepsilon)$ terms, it follows that $\dot{d}_{n-2} = 0$ and $d_{n-1} = r_{n-3}$, we get from (4.13) that

$$\dot{d}_{n-1} \sim -\frac{2}{d_{n-2}^0(s_+ - s-)^2} a_{n-1}^2 \nu_{n-1}^2 e^{-\varepsilon^{-1}\nu_{n-1}d_{n-1}}\,, \qquad d_{n-1}(0) = d_{n-1}^0\,, \tag{4.15}$$

where $d_{n-2}^0 = d_{n-2}(0)$. The solution to this ODE is

$$d_{n-1}(t) \sim d_{n-1}^0 + \frac{\varepsilon}{\nu_{n-1}} \log\left(1 - t/t_s\right)\,, \qquad t_s \equiv \frac{\varepsilon(s_+ - s_-)^2}{2a_{n-1}^2\nu_{n-1}^3} d_{n-2}^0\, e^{\varepsilon^{-1}\nu_{n-1}d_{n-1}^0}\,. \tag{4.16}$$

Hence $d_{n-1}(t) = 0$, when $t = t_s + O(1)$. The case with $J = 1$ is similar.

Finally, we consider the case where $J = n$. In this case, we obtain from (3.8e) and (3.7d) that

$$r_{n-2} \sim \frac{2}{d_{n-1}(s_+ - s_-)^2}\, a_n^2 \nu_n^2\, e^{-\varepsilon^{-1}\nu_n d_n}\,, \tag{4.17}$$

and $r_j = o'(r_{n-2})$ for all $j = 0, \ldots, n$ with $j \neq n-2$. Thus, we obtain from (3.11) that

$$\dot{x}_{n-2} \sim r_{n-2}\,; \quad \dot{x}_{n-1} \sim r_{n-2}\,; \quad \dot{x}_j \sim \varepsilon^{n-2-j} r_{n-2}\omega_j\,, \qquad 0 \leq j \leq n-3\,, \tag{4.18}$$

for some $\omega_j > 0$. Thus, the layers x_{n-2} and x_{n-1} will move to the right at the same speed r_{n-2}, while the other layers move in the same direction, but at an algebraically slower speed in ε. This is verified in Figs. 6(a), (b). In a similar way as in the derivation of (4.16) we obtain

$$x_{n-1}(t) \sim x_{n-1}(0) - \frac{\varepsilon}{2\nu_n}\log(1-t/t_s)\,, \qquad t_s \equiv \frac{\varepsilon(s_+-s_-)^2}{4a_n^2\nu_n^3} d_{n-1}^0\, e^{2\varepsilon^{-1}\nu_n(1-x_{n-1}^0)}\,, \tag{4.19}$$

where $d_{n-1}^0 = d_{n-1}(0)$ and $x_{n-1}^0 = x_{n-1}(0)$. Notice that the collapse time t_s is very different from the corresponding collapse time for the viscous case given in (4.7).

4.3 The Simultaneous Collapse of a Pair of Intervals

Next, we consider the dynamics of an n-layer metastable pattern which has two smallest neighboring intervals. Specifically, we assume that $n \geq 4$ and that there is some J with $2 \leq J \leq n-2$ such that $\nu_J d_J^0 = \nu_{J+1} d_{J+1}^0 < \nu_j d_j^0$ for all $j = 0, \ldots, n$ and $j \neq J, J+1$. For the sake of simplicity, we let $Q(u)$ be an odd nonlinearity for which $a_+ = a_- \equiv a$ and $\nu_+ = \nu_- \equiv \nu$. In this case, $d_J^0 = d_{J+1}^0$. We then look for a solution where $d \equiv d_J \sim d_{J+1}$ as $\varepsilon \to 0$ during the metastable phase. Defining $H \equiv 2a^2\nu^2\, e^{-\varepsilon^{-1}\nu d}$, we obtain from (2.13a) that $H_{J-1} \sim H$, $H_{J+1} \sim -H$, and $H_j = o'(H)$ for all $j = 0, \ldots, n$ with $j \neq J-1$ and $j \neq J+1$.

For the viscous case with $0 < \alpha \leq 1$ we find from (3.5a) that

$$\alpha\kappa\beta\dot{x}_{J-1} \sim \varepsilon H_{J-1} > 0\,; \qquad \alpha\kappa\beta\dot{x}_{J+1} \sim \varepsilon H_{J+1} < 0\,; \qquad \dot{x}_j = o'(H)\,, \qquad j \neq J-1,\, J+1\,. \tag{4.20}$$

Thus, during the metastable phase the layers x_{J-1} and x_{J+1} move towards each other, while the other layers, including the interface x_J joining the smallest intervals (x_{J-1}, x_J) and (x_J, x_{J+1}), remains essentially stationary in time. This behavior is seen clearly in Figs. 7(c)–(f).

For the Cahn-Hilliard equation ($\alpha = 0$), it is easy to show from (3.8e) and (3.7d) that

$$\begin{aligned} r_{J-2} &\sim \frac{1}{d_{J-1}(s_+-s_-)^2}\, H_{J-1}\,, \qquad r_{J-1} \sim \frac{1}{d_J(s_+-s_-)^2}\, H_{J-1}\,, \\ r_J &\sim \frac{1}{d_{J+1}(s_+-s_-)^2}\, H_{J+1}\,, \qquad r_{J+1} \sim \frac{1}{d_{J+2}(s_+-s_-)^2}\, H_{J+1}\,, \\ r_j &= o'(H)\,, \qquad \text{for } j \neq J\pm 1,\, J\pm 2\,. \end{aligned} \tag{4.21}$$

Therefore, from the leading term in (3.11a), we find that the internal layer locations $x_j(t)$ satisfy

$$\begin{aligned} \dot{x}_{J-2} &\sim r_{J-2} > 0\,, \qquad \dot{x}_{J-1} \sim r_{J-1} + r_{J-2} > 0\,, \\ \dot{x}_{J+2} &\sim r_{J+1} < 0\,, \qquad \dot{x}_{J+1} \sim r_J + r_{J+1} < 0\,, \\ \dot{x}_j &= O(\varepsilon H)\,, \qquad \text{for } j \neq J\pm 1,\, J\pm 2\,. \end{aligned} \tag{4.22}$$

Here we have to assume $d^0_{J-1} = d^0_{J+2}$ in order to ensure that our former assumption $d_J \sim d_{J+1}$ is valid. Therefore, the internal layers whose motion is most noticeable during the metastable phase are x_{J-2}, x_{J-1} that move to the right and x_{J+1}, x_{J+2} that move to the left. The other layers remain stationary to within at least $O(\varepsilon)$ precision. In addition, from (4.21), it is clear that $x_{J\pm1}$ moves more quickly than does $x_{J\pm2}$. The numerical evidence supporting this analysis is observed in Figs. 7(a), (b).

4.4 Comparison with Other ODE Systems

A system of ODE's for the Cahn-Hilliard equation has been derived in [6] and [12] and it is of interest to compare these systems with (3.11). In our notation, the ODE system of Bates and Xun (equation [4.36] in [6]) can be rewritten as

$$\dot{x}_j \sim r_j + r_{j-1}\,, \quad \text{for } 1 \le j \le n-2\,, \qquad \dot{x}_0 \sim r_0\,, \qquad \dot{x}_{n-1} \sim r_{n-2}\,. \tag{4.23}$$

Thus, $\dot{\mathbf{x}} \sim \dot{\mathbf{x}}^0$, where $\dot{\mathbf{x}}^0$ is the leading term in (3.11). Therefore, the results in [6] provide a description of the motion of the internal layers corresponding to the annihilating interval and its two nearest neighbors, but they may be inaccurate for other layers. For example, suppose J with $2 \le J \le n-2$ and $n \ge 4$ is the index of a unique annihilating interval. Then, our asymptotic expansion (3.11) indicates that the internal layers x_j for $j = J-k$ with $k \ge 2$ and $j = J+k$ with $k \ge 1$ will move at an algebraic slower speed in ε than the annihilating layers. On the other hand, from (4.23), the corresponding internal layers x_j will satisfy $\dot{x}_j = o'(\dot{x}_J)$, i.e., they move exponentially slower than the collapsing layers. Similarly, for the case corresponding to Figs. 6(a), (b), where the annihilating interval is $(x_{n-1}, 1)$, the system (4.23) yields $x_j' = o'(r_{n-1})$ for $j \le n-3$. In contrast, our ODE system (3.11) gives (4.18) instead. In Table 6, corresponding to Figs. 6(a) and (b), we illustrate that (4.18) is correct by giving the numerical results for the locations x_j, their deviations $e_j \equiv x_j - x_j^0$ from their initial values, and the ratios $\rho_j \equiv e_j/e_{j+1}$ at two different times. These results are computed from the full problem (2.1) using the TMOL method. From (4.18), we expect that the ratio ρ_j with $j \le n-3$ should be $O(\varepsilon)$, and that the deviation e_j should satisfy $O(\varepsilon^{n-2-j} e_{n-2})$ for $j \le n-3$. This is exactly what is obtained in Table 6.

Eyre [12] also derived an explicit ODE system for the Cahn-Hilliard equation using a collocation technique. However, we can't find any similarities between his results and our asymptotic results.

4.5 The Behavior of σ During a Collapse

We now explain a prominent phenomenon observed in Figs. 3–7. These figures show that for the viscous case with $0 < \alpha \le 1$, the value of u in the intervals that are not collapsing will deviate some visible vertical distance from the original positions $u \sim s_\pm$. This deviation, however, does not occur during the coarsening

	$t = 140.22$			$t = 156.02$		
j	x_j	e_j	ρ_j	x_j	e_j	ρ_j
0	-.800000	.000000	-	-.800000	.000000	-
1	-.499998	.000002	.05	-.499995	.000005	.04
2	-.099961	.000039	.05	-.099861	.000139	.05
3	.200718	.000718	.04	.202578	.002578	.04
4	.617812	.017812	1.04	.671481	.071481	.81
5	.917114	.017114		.987852	.087852	

Table 6: Numerical results (using TMOL) for the Cahn-Hilliard equation ($\alpha = 0$) at two different times corresponding to the parameter values used for Figs. 6(a) and (b). Here, x_j for $j = 0, \ldots, 5$ are the locations of the internal layers, $e_j \equiv x_j - x_j^0$ and $\rho_j \equiv e_j/e_{j+1}$.

process for the Cahn-Hilliard equation. Since u should be constant when $Q(u) - \sigma = 0$, as seen from (2.1a), we anticipate that this shifting behavior results from the different signs and values of $\sigma(x,t)$ for the different models. Specifically, we can expect that if $\sigma < 0$ ($\sigma > 0$), then the the top of an "island" and the bottom of an "valley" will shift up (down), and furthermore, the deviated distance will depend on the value of σ.

We now derive asymptotic expressions for $\sigma(x,t)$ for the different models to interpret this difference. The formula for $\sigma(x,t)$ is given in (2.8), where $M_j(x;x_j)$ in (2.8b) satisfies

$$M_j = O(e^{-\varepsilon^{-1}c}) \quad \text{for } x < x_j\,; \qquad M_j \sim \xi_j(s_+ - s_-)(x - x_j) \quad \text{for } x > x_j\,. \tag{4.24}$$

Here $c > 0$ is proportional to the distance $|x - x_j|$. The function $\sigma_c(t)$ in (2.8a) is given in (3.5a) for the viscous case $0 < \alpha \leq 1$ and in (3.11b) for the Cahn-Hilliard equation $\alpha = 0$.

Consider the viscous case with $n \geq 3$ and assume that the interval (x_{J-1}, x_J) is the unique collapsing interval, with $1 \leq J \leq n-1$. Then from (2.13a),

$$H_{J-1} \sim H\,, \qquad H_J \sim -H\,, \quad \text{where} \quad H \equiv 2a_J^2\nu_J^2\, e^{-\varepsilon^{-1}\nu_J d_J}\,, \tag{4.25}$$

and $H_j = o'(H)$ for all $j = 0, \ldots, n$ with $j \neq J$ and $j \neq J-1$. Using the leading term in (3.5a) we determine σ_c. Then, from (2.8) we get

$$\sigma = \sigma_c\,[1 + (1-\alpha)O(\varepsilon)]\,, \qquad \sigma_c \sim 2\,\xi_J\, n^{-1}(s_+ - s_-)^{-1}H\,. \tag{4.26}$$

Therefore, the leading order behavior of σ_c is the same for the constrained Allen-Cahn equation $\alpha = 1$ as it is for the viscous Cahn-Hilliard equation $0 < \alpha < 1$. If $\xi_J < 0$, then $\sigma < 0$ and the value of u in the non-collapsing intervals will shift up. If $\xi_J < 0$, it shifts down. This analysis agrees with the numerical

results shown in Figs. 3–7. For example, in Fig. 3 and 4, $\xi_J = -1$ with $J = 3$ and $\sigma_c < 0$. Thus, the metastable pattern on the intervals not involved in the collapse is lifted up during the coarsening process.

We now contrast this result with the Cahn-Hilliard equation. Let $n \geq 4$ and assume that for some J with $2 \leq J \leq n-2$ the unique collapsing interval is (x_{J-1}, x_J). Then, using (3.11), (4.24) and (4.25), we can calculate $\sigma(x,t)$ in each interval (x_{k-1}, x_k), with the result

$$\sigma(x,t) \sim -\xi_k H \varepsilon^{J-k-1} \omega_k\,, \quad \text{on} \quad x_{k-1} < x < x_k\,, \quad \text{with} \quad 0 \leq k \leq J-1\,, \tag{4.27a}$$

$$\sigma(x,t) \sim \xi_J H \omega_k\,, \quad \text{on} \quad x_{k-1} < x < x_k\,, \quad \text{with} \quad J-1 \leq k \leq J+1\,, \tag{4.27b}$$

$$\sigma(x,t) \sim -\xi_k H \varepsilon^{k-J-1} \omega_k\,, \quad \text{on} \quad x_{k-1} < x < x_k\,, \quad \text{with} \quad J+1 \leq k \leq n\,. \tag{4.27c}$$

Here $\omega_k > 0$ is an $O(1)$ constant. Thus, as $d_J \to 0$, H becomes $O(1)$ and $\sigma(x,t)$ becomes $O(1)$ in the annihilating interval and its left and right nearest neighbors. However, $\sigma(x,t)$ will be $O(\varepsilon^k)$ in intervals which are $k+1$ intervals either to the right or to the left of the collapsing interval (x_{J-1}, x_J). Thus, for these intervals, the shifts in the height of u should be negligible. This is clearly observed in the numerical results shown in Fig. 2, Figs. 5(a)–(b), Figs. 6(a)–(b).

5 Simulation of the Entire Coarsening Process

The DAE system (2.12) is not valid when two internal layers, or an internal layer and a wall, become closely separately by an amount of $O(\varepsilon)$. In particular, when two approaching internal layers become closely separated, the layers will undergo a strong local interaction which leads to an annihilation of two internal layers, leaving behind a metastable pattern with two fewer layers. This strong local interaction of two approaching internal layers during annihilation is very complicated (see Fig. 2-7) and will not be discussed. Instead, we will find an approximation of the interface realignment after an annihilation, using the explicit characterization of the layer motion described in the previous section. Here interface realignment refers to an algorithm that maps interface locations before an annihilation to locations immediately after an annihilation. Since an annihilation event takes place on a much faster time scale than metastable dynamics, we believe that incorporating the interface realignment into the metastable evolution described by the DAE system (2.12) could provide, approximately, a complete quantitative description of the coarsening process associated with the phase separation models.

In our discussion below, we assume that at any time, the interval having the least length is unique, i.e., there is some J with $0 \leq J \leq n$ such that $\nu_J d_J < \nu_j d_j$ for all $j = 0, \ldots, n$ and $j \neq J$. Another assumption is that the solution $u(x,t)$ is a piecewise constant with $u = s_+$ or $u = s_-$ during the metastable phase. This is reasonable since when ε is small, the extent over which u in (2.2) is not piecewise constant

is $O(\varepsilon)$. Under this assumption, the mass constraint is equivalent to the conservation conditions that the sum of the lengths of the regions where $u = s_+$ or where $u = s_-$ in (2.2) remains constant in time. Since the interval with the least length annihilates first, the layers x_{J-1} and x_J will be referred to as the left and right annihilating interfaces, while the layers x_{J-2} and x_{J+1} will be referred to as the left and right nearest interfaces. During the annihilation of the J-th interval, the interface number decreases by two (one if $J = 0$ or n). Let the locations of the resulting interfaces immediately after the annihilation be denoted by $\tilde{x}_j$ for $j = 0, \ldots, J-2, J+1, \ldots, n-1$, where we assume that the set $\{0, \ldots, J-2\}$ ($\{J+1, \ldots, n-1\}$) is empty if $J < 2$ ($J > n-2$). As in §4, there are two ranges of α that need to be considered. We first consider the viscous case.

5.1 The Viscous Case: $0 < \alpha \leq 1$

Assume that J, with $J \neq 0$ and $J \neq n$, is the index of the only annihilating interval. It has been shown in §4 that the annihilating interfaces approach each other and eventually coalesce, while the remaining interfaces move at a common speed and in alternating directions. Thus, the new locations of the internal layers after an annihilation can be approximated by

$$\tilde{x}_j = x_j + (-1)^{j-J}\delta\,, \qquad j = 0, \ldots, n-1, \;\; j \neq J-1, J\,, \tag{5.1}$$

where $\delta > 0$ is a constant. Using the length conservation conditions, we have $\delta = d_J/(n-2)$. If $J = 0$ or n, then the new internal layer locations after an annihilation can be approximated by

$$\tilde{x}_j = x_j + (-1)^{j-J}\delta\,, \qquad j = 0, \ldots, n-1, \;\; j \neq (1 - \frac{1}{n})J\,, \tag{5.2}$$

with $\delta = d_J/2(n-1)$.

5.2 The Cahn-Hilliard Equation: $\alpha = 0$

In this case, the asymptotic analysis and numerical experiments in §4 showed that when $2 \leq J \leq n-2$ ($n \geq 4$), the nearest interfaces x_{J-2} and x_{J+1} will move at the same speeds and directions as the corresponding annihilating interfaces x_{J-1} and x_J, while all other interfaces remain stationary to within at least $O(\varepsilon)$ precision. Thus, the new locations of the interfaces can be approximately represented by

$$\tilde{x}_{J-2} = x_{J-2} + \delta d_J\,, \qquad \tilde{x}_{J+1} = \tilde{x}_{J-2} + d_{J-1} + d_{J+1}\,, \tag{5.3a}$$

$$\tilde{x}_j = x_j\,, \qquad j = 0, \ldots, J-3, J+2, \ldots, n-1\,. \tag{5.3b}$$

Here $\delta > 0$ is a constant to be determined. To find an approximation for δ, we compare the speeds of the nearest interfaces during the metastable phase. It is clear from (4.9) that the annihilating interfaces move

towards each other, each being followed by its nearest interface moving at approximately the same speed. The ratio of the speeds of these two rigid motions is equal to the inverse ratio of the distances between the pairs of the nearest and annihilating interfaces. Thus, we obtain

$$\delta = \frac{d_{J+1}}{d_{J-1} + d_{J+1}}. \tag{5.4}$$

Note that if $d_{J-1} = d_{J+1}$, then $\delta = \frac{1}{2}$ and the length of the annihilated interval is redistributed equally to its neighboring intervals. The discussion above is limited to the case of annihilating intervals that are separated from the boundary by at least two intervals. When the annihilating interfaces are near the boundary, it is not hard to see from (4.14) and (4.18) that if $J = n-1$ or $J = n$, then the interface(s) x_j for $J-1 \le j \le n-1$ will eventually disappear. Since, during this annihilation, the interfaces x_j for $0 \le j \le J-2$ are almost stationary, the new location of the left nearest interface x_{J-2} can be calculated using the length conservation condition. Specifically, we have

$$\tilde{x}_{n-3} = x_{n-1} - d_{n-2}\,, \quad \tilde{x}_j = x_j\,, \quad \text{for } j = 0, \ldots, n-4\,, \quad \text{if } J = n-1, \tag{5.5a}$$

$$\tilde{x}_{n-2} = 1 - d_{n-1}\,, \qquad \tilde{x}_j = x_j\,, \quad \text{for } j = 0, \ldots, n-3\,, \quad \text{if } J = n\,. \tag{5.5b}$$

The interface realignment for $J = 0$ or 1 can be implemented similarly. Our discussions here are motivated by the work of Eyre [12] for the Cahn-Hilliard equation. Comparing (5.3)-(5.5) with the corresponding equations for the interface motion during annihilation given in [12], we find they are essentially equivalent.

5.3 The Realignment Algorithm

Finally, we present the realignment algorithm that is used to approximately describe the entire coarsening process associated with our phase separation models. We first integrate the DAE system (2.12) until a collapse criterion is satisfied. Then we use the interface realignment technique to determine the new locations of the interfaces after an annihilation. With these new interface locations as initial values, we return to integrate the DAE system again. We repeat the procedure above for each successive collapse event until a stable equilibrium state with only one internal layer is achieved. This final configuration has, to within $O(\varepsilon)$ terms, the same mass as the initial data. Using this procedure, we calculate and plot in Fig. 8 the interface locations as a function of time for the Cahn-Hilliard equation ($\alpha = 0$) and for the constrained Allen-Cahn equation ($\alpha = 1$). This figure shows the entire coarsening process associated with these phase separation models and the two distinct time scales of the fast annihilation and the metastable interface motion.

Acknowledements

M.J.W. is grateful for the hospitality of the Chinese University of Hong Kong where much of this paper was written, and to Prof. Michele Schatzmann for providing us with the reference [12].

References

[1] N. Alikakos, P.W. Bates, G. Fusco, *Slow motion for the Cahn-Hilliard equation in one space dimension*, J. Diff. Equat. **90**, (1991), pp. 81–135.

[2] U. Ascher, R. Christiansen, R. Russell, *Collocation software for boundary value ODE's*, Math. Comp. **33**, (1979), pp. 659–679.

[3] U. Ascher, R. Mattheij, R. Russell, *Numerical solution of boundary value problems for ordinary differential equations.* Englewood Cliffs, N.J., Prentice Hall, 1988.

[4] F. Bai, C.M. Elliott, A. Gardiner, A. Spence, A.M. Stuart, *The viscous Cahn-Hilliard equation. Part I: computations.* Nonlinearity **8**, (1995), pp. 131–160.

[5] F. Bai, A. Spence, A.M. Stuart, *Numerical computations of coarsening in the one-dimensional Cahn–Hilliard model of phase separation*, Physica D **78**, (1994), pp. 155-166.

[6] P.W. Bates, J. Xun, *Metastable patterns for the Cahn-Hilliard equation: part 1 and 2*, J. Diff. Equat. **111**, (1994), pp. 421–457; J. Diff. Equat. **117**, (1995), pp. 165–216.

[7] L. Bronsard, D. Hilhorst, *On the slow dynamics for the Cahn-Hilliard equation in one space dimension*, Proc. Roy. Soc. London A. **439**, (1992), pp. 669–682.

[8] J.W. Cahn, J.E. Hilliard, *Free energy of a nonuniform system. I. Interfacial free energy*, J. Chem. Phy. **28**, (1958), pp. 258–267.

[9] J. Carr, R. Pego, *Metastable patterns in solutions of* $u_t = \varepsilon^2 u_{xx} - f(u)$, Comm. Pure Appl. Math. **42**, (1989), pp. 523–576.

[10] J.R. Cash, *The integration of stiff initial value problems in ODEs using modified extended backward differentiation formulae*, Comput. Math. Appl. **9** (1983), pp. 645–657.

[11] C.M. Elliott, D.A. French, *Numerical studies of the Cahn–Hilliard equation for phase separation*, IMA J. Appl. Math. **38**, (1987), pp. 97–128.

[12] D.J. Eyre, *Coarsening dynamics for solutions of the Cahn-Hilliard equation in one dimension*, unpublished, (1992).

[13] G. Fusco, J.K. Hale, *Slow motion manifolds, dormant instability and singular perturbations*, J. Dyn. Diff. Equat. **1**, (1989), pp. 75–94.

[14] C. Grant, *Slow motion in one-dimensional Cahn-Morral systems*, SIAM J. Math. Anal. **26**, (1995), pp. 21–34.

[15] A.C. Hindmarsh, *Odepack, a systematized collection of ode solvers*, in Scientific Computing, R.S. Stepleman, et al. (eds.), North-Holland, Amsterdam, 1983, pp. 55-64.

[16] W. McKinney, *Ph.D. Thesis*, Dept. of Math., U. of Tennesse, Knoxville (1989).

[17] J. Neu, unpublished notes, (1984).

[18] A. Novick-Cohen, *On the viscous Cahn-Hilliard equation*, In: Material Instabilities in Continuum Mechanics and Related Mathematical Problems (J. Ball, editor), Oxford Sci. Publ., Oxford Univ. Press, New York, 1988, pp. 329–342.

[19] L.G. Reyna, M.J. Ward, *Resolving weak internal layer interactions for the Ginzburg-Landau equation*, European J. Appl. Math. **5**, (1994), pp. 495–523.

[20] L.G. Reyna, M.J. Ward, *Metastable internal layer dynamics for the viscous Cahn-Hilliard equation*, Methods and Appl. of Anal. **2**, No. 3, (1995), pp. 285–306.

[21] J. Rubinstein, P. Sternberg, *Nonlocal reaction-diffusion equations and nucleation*, IMA J. Appl. Math. **48**, (1992), pp. 249–264.

[22] M.J. Ward, *Metastable patterns, layer collapses, and coarsening for a one–dimensional Ginzburg-Landau equation*, Stud. Appl. Math. **91**, (1994), pp. 51–93.

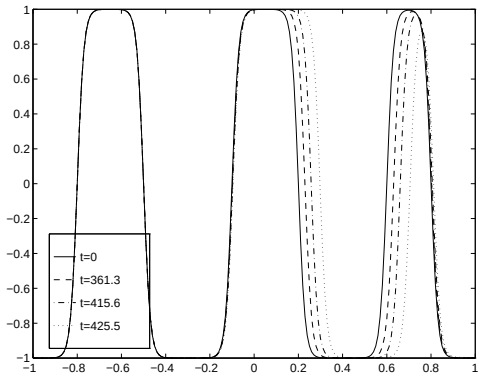

(a): $\alpha = 0\,,\ \varepsilon = 0.03$

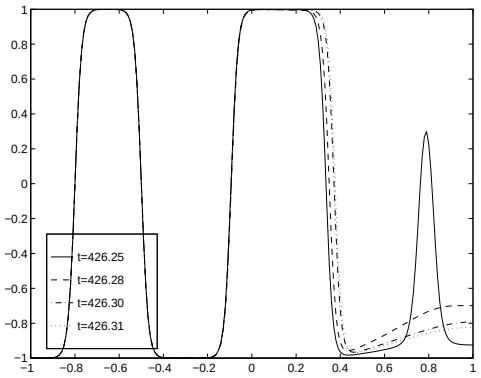

(b): $\alpha = 0\,,\ \varepsilon = 0.03$

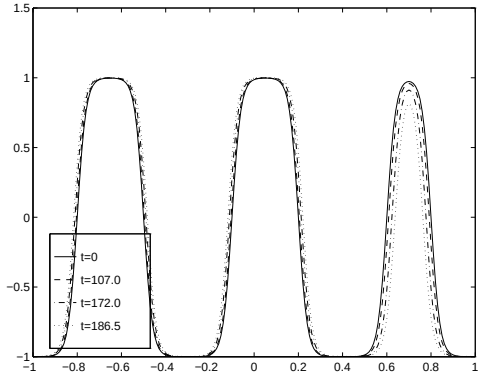

(c): $\alpha = 0.5\,,\ \varepsilon = 0.04$

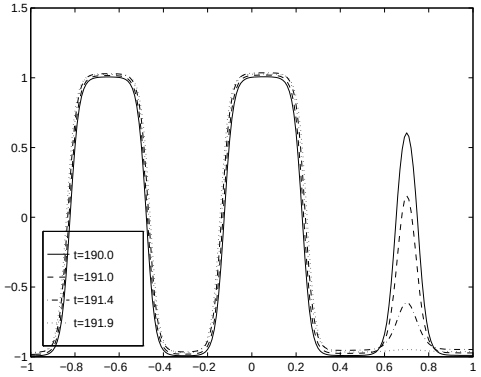

(d): $\alpha = 0.5\,,\ \varepsilon = 0.04$

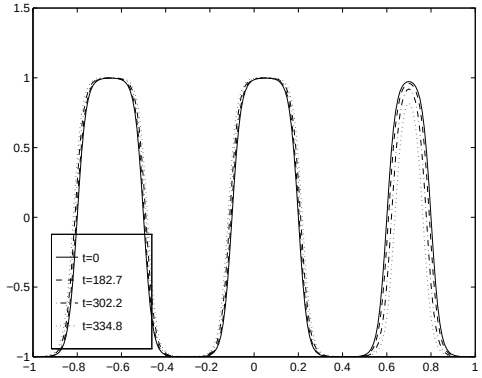

(e): $\alpha = 1\,,\ \varepsilon = 0.04$

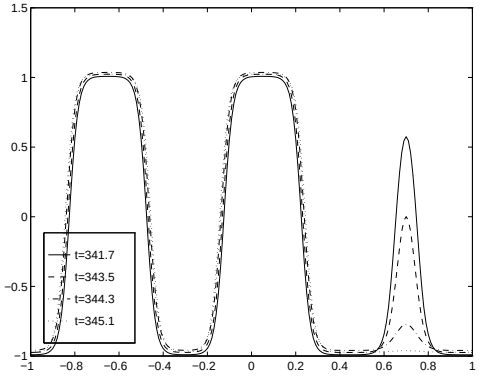

(f): $\alpha = 1\,,\ \varepsilon = 0.04$

Figure 5: Plots of the full numerical solutions (using TMOL) to (2.1) at different times for various values of α and ε. The initial data is $u(x,0) \equiv u^*(x;\boldsymbol{x}^0)$ with $\boldsymbol{x}^0 = (-0.8,\ -0.5,\ -0.1,\ 0.2,\ 0.6,\ 0.8)$ and u^* defined by (2.2).

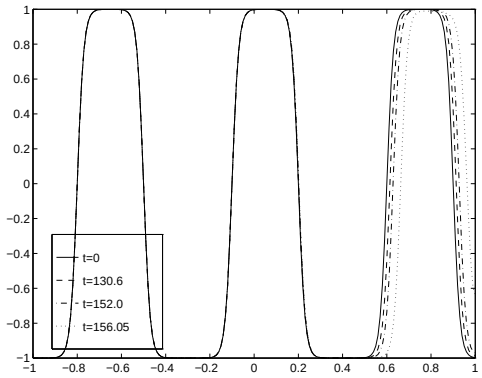

(a): $\alpha = 0\,,\ \varepsilon = 0.03$

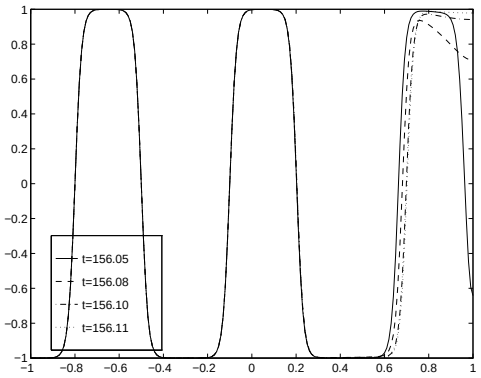

(b): $\alpha = 0\,,\ \varepsilon = 0.03$

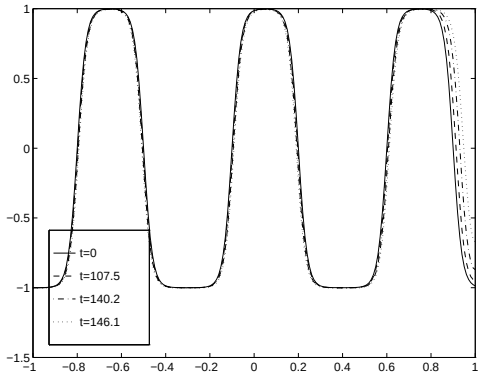

(c): $\alpha = 0.5\,,\ \varepsilon = 0.04$

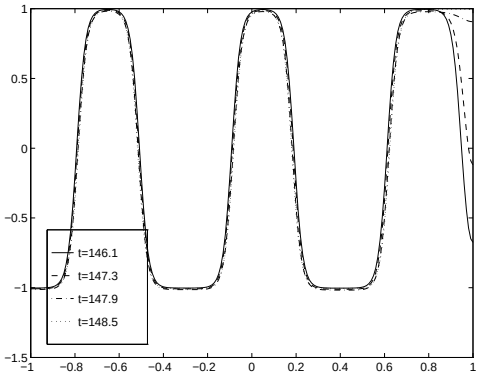

(d): $\alpha = 0.5\,,\ \varepsilon = 0.04$

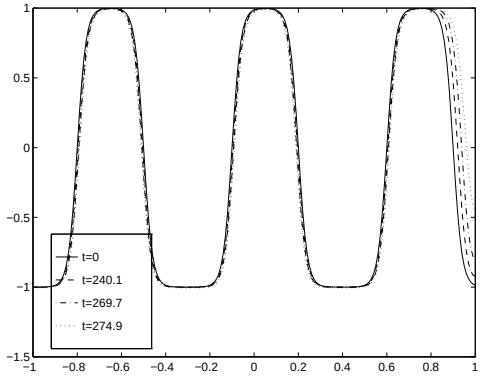

(e): $\alpha = 1\,,\ \varepsilon = 0.04$

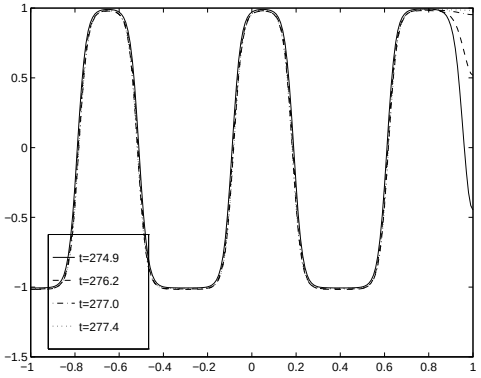

(f): $\alpha = 1\,,\ \varepsilon = 0.04$

Figure 6: Plots of the full numerical solutions (using TMOL) to (2.1) at different times for various values of α and ε. The initial data is $u(x,0) \equiv u^*(x;\boldsymbol{x}^0)$ with $\boldsymbol{x}^0 = (-0.8,\ -0.5,\ -0.1,\ 0.2,\ 0.6,\ 0.9)$ and u^* defined by (2.2).

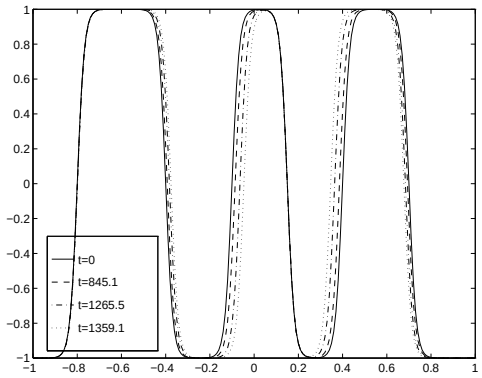

(a): $\alpha = 0\,,\ \varepsilon = 0.032$

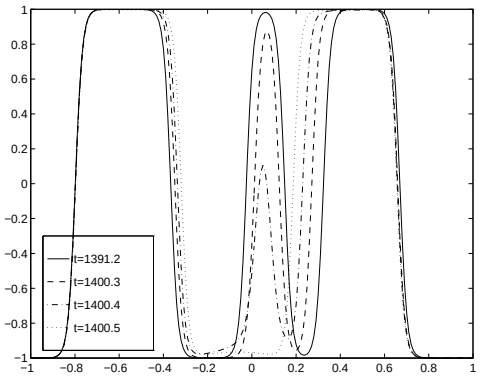

(b): $\alpha = 0\,,\ \varepsilon = 0.032$

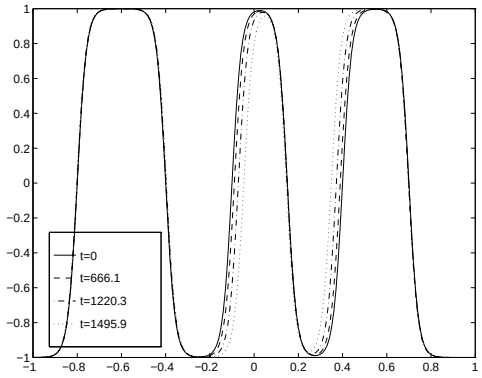

(c): $\alpha = 0.5\,,\ \varepsilon = 0.042$

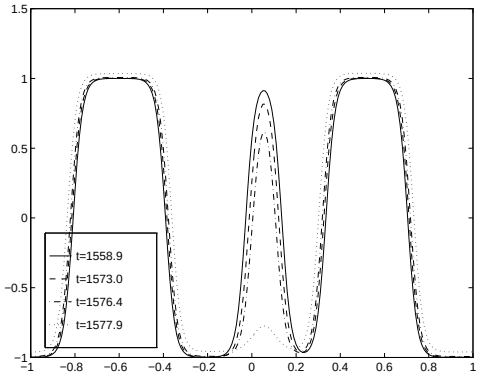

(d): $\alpha = 0.5\,,\ \varepsilon = 0.042$

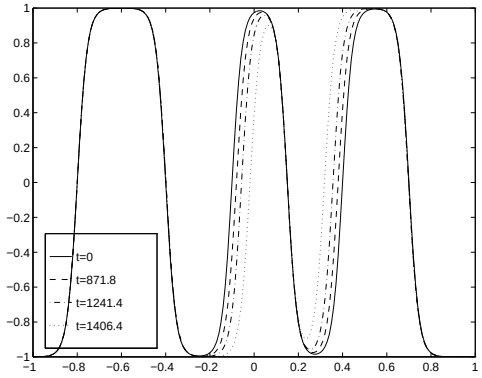

(e): $\alpha = 1\,,\ \varepsilon = 0.045$

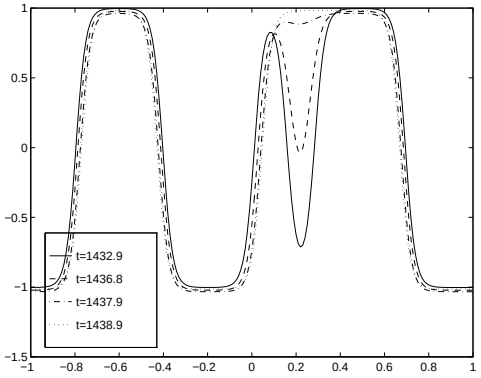

(f): $\alpha = 1\,,\ \varepsilon = 0.045$

Figure 7: Plots of the full numerical solutions (using TMOL) to (2.1) at different times for various values of α and ε. The initial data is $u(x,0) \equiv u^*(x;\boldsymbol{x}^0)$ with $\boldsymbol{x}^0 = (-0.8,\ -0.4,\ -0.1,\ 0.15,\ 0.4,\ 0.7)$ and u^* defined by (2.2).

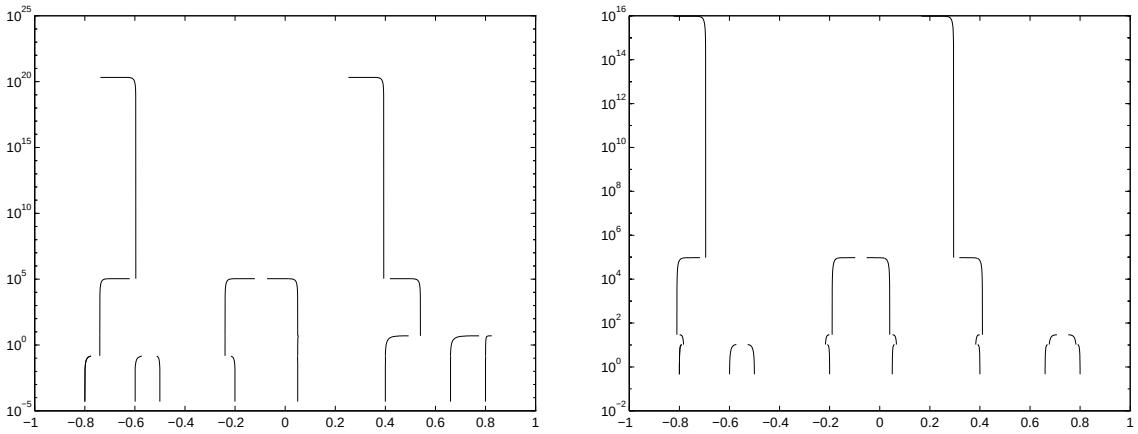

(a) $\alpha = 0$ (b) $\alpha = 1$

Figure 8: Plots of the interface locations as a function of time for (2.1) with $\varepsilon = 0.02$. Here the initial locations of the interfaces are –0.8, –0.6, –0.5, –0.2, 0.05, 0.4, 0.66, 0.8, and the final stable equilibrium having one interface at $x_0 = -0.01$ is achieved at $t \sim .2096 \times 10^{21}$ for the Cahn-Hilliard equation where $\alpha = 0$ and at $t \sim .9551 \times 10^{16}$ for the constrained Allen-Cahn equation where $\alpha = 1$.